batteries

MDPI

Review

Binder Alternatives and Manufacturing Challenges in Emerging Lithium Battery Technologies

Junzheng Li [1] and Shiladitya Paul [2,3,*]

[1] St Edmund's College, University of Cambridge, Cambridge CB3 0BN, UK; jzl27@cam.ac.uk
[2] Metallic Materials & Integrity Technology Group, TWI, Cambridge CB21 6AL, UK
[3] Materials Innovation Centre, School of Engineering, University of Leicester, Leicester LE1 7RH, UK
* Correspondence: shiladitya.paul@twi.co.uk

Abstract

The need for the rapid advancement of lithium-based energy storage technologies continues to outpace progress in materials development and manufacturing, creating a widening gap between laboratory-scale innovation and industrial deployment. There is a need to examine the key materials and processing challenges that limit the performance, cost-effectiveness, and sustainability of next-generation lithium batteries. For material considerations, many commonly used electrodes face issues of volumetric expansion and performance degradation over charging cycles. To address these issues, binders are a crucial component to consider as they adhere active materials to the electrodes, and their structure can be altered to mitigate undesirable effects from these components. Hence, the selection and exploration of alternative binders are becoming increasingly important in the pursuit of longer-lasting and safer Li-batteries. From a manufacturing perspective, current production lines rely on multistep, energy-intensive processes, e.g., from slurry-mixing to cell assembly, that elevate costs and complicate scale-up. Emerging chemistries incorporating nanomaterials or solid-state components face additional barriers related to yield, process control, and defect management, all of which can exacerbate safety risks related to processing during production and thermal runaway in produced batteries. End-of-life considerations, including disassembly, recycling, and the safe handling of toxic materials, further contribute to the technological and logistical complexity of large-scale deployment. The field is moving toward sustainable material alternatives, more efficient and adaptive manufacturing routes, and advanced technologies such as solid-state electrolytes and nanostructured electrodes. Together, these developments provide a roadmap for overcoming current bottlenecks and enabling the next generation of high-performance, safe, and sustainable lithium battery technologies. This review examines the progress made in finding alternative materials and synthesis methods for the optimization of lithium battery cells, with a focus on the development of novel binders, slurry synthesis and manufacturing framework. In addition, the advantages and limitations of the alternative binder materials and processes are also explored, with a focus on scalability for manufacturing, safety concerns, sustainability and end-of-life challenges.

Keywords: lithium-ion batteries; lithium sulfur batteries; binders; manufacturing; recycling; safety; circular economy

Academic Editor: Xianyong Wu

Received: 16 April 2026
Revised: 16 May 2026
Accepted: 22 May 2026
Published: 25 May 2026

1. Introduction

It is well-established that greenhouse gas (GHG) emissions, pollution, and reliance on fossil fuels result in global warming and climate change, leading to concerns and hence

emphasizing the need for the development and usage of renewable energy [1,2]. However, renewable energy sources face issues of inconsistency [3], and hence efficient energy storage is crucial for a thorough and effective transition to renewable energy [4]. With the shift from internal combustion (IC) engine-based vehicles to electrical vehicles (EVs) in recent years, Li-ion batteries have become a prominent option for EV applications due to their reasonable energy density and life cycle [3]. As a result, research on lithium-ion batteries (LIBs) has been growing [5] due to their widespread application not just in electric vehicles, but also in portable devices and electrochemical storage [6,7]. The global lithium-ion battery market is anticipated to expand from USD 68.66 billion in 2025 to USD 306.24 billion by 2033, reflecting substantial and accelerating industry growth [8]. However, commercial LIBs often have limited energy density and are unable to satisfy the requirements of the current market [7]. Additionally, traditional industrial production consumes large amounts of solvents, which leads to issues regarding energy waste, volatile organic content (VOC)-related safety and pollution [9]. Hence, it is important to incorporate environmental and large-scale feasibility considerations into assessments of the various novel materials investigated for LIB components.

The structure of a lithium-ion battery is mainly composed of a positive electrode, negative electrode, separator, electrolyte, and packaging materials (Figure 1a,b) [10]. Within each electrode, active materials, conductive additives, are adhered to the current collector with the use of binders. (Figure 2). These polymeric binders ensure that the connections of solid–solid interfaces between these components are tight and stable [11].

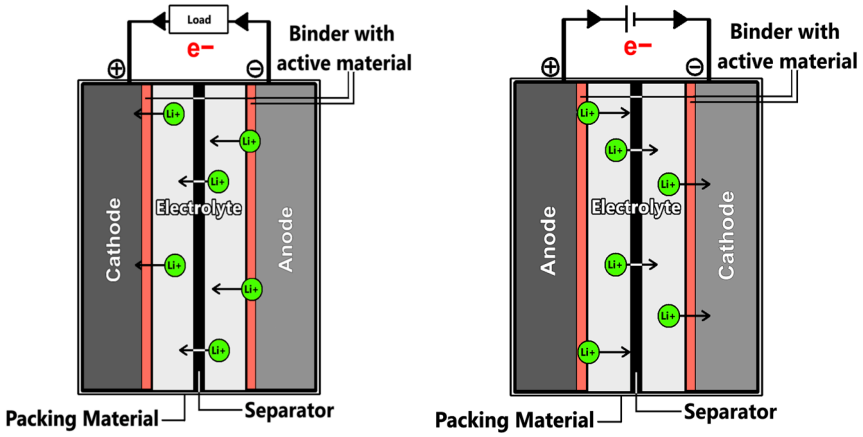

Figure 1. Diagrams illustrating the movement of lithium ions (**a**) during discharge and (**b**) during charging, demonstrating the rechargeable nature of Li batteries. (Inspired by P.U. Nzereogu et al. [12]). This is a simplified diagram and only the key components are shown. Current collectors, metal foils, additives, casing, sealing systems, etc., are not shown.

Lithium-ion battery operation relies on the reversible intercalation and deintercalation of lithium ions (Li^+) between a cathode and an anode (Figure 3). During charge and discharge cycles, the electrolyte facilitates the internal migration of Li^+ ions, while electrons synchronously travel through an external circuit to maintain charge neutrality [5]. Various materials are explored for suitable cathodes, such as $LiMn_2O_4$ [13], $LiCoO_2$, $LiFePO_4$ and Ni-Co-Mn, while common anode materials include carbon-based ones such as graphene [14], alloys, and transitional metal oxides [15]. The intercalation, conversion, and alloy formation that occur at the electrode–electrolyte interface are the main processes that determine the energy storage of the battery [16].

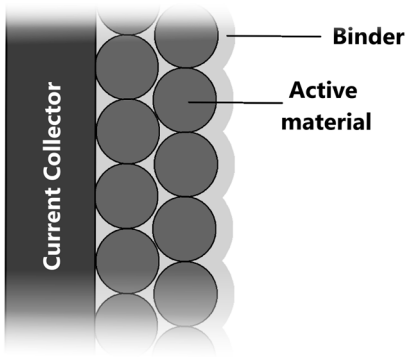

Figure 2. Diagram illustrating the zoomed-in structure of an electrode along its surface and the general functions of the binder. This is a simplified schematic for visualization.

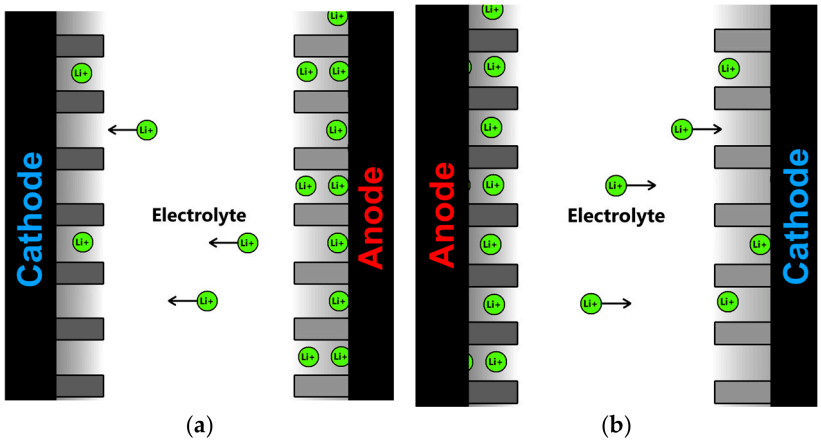

Figure 3. Diagram illustrating the process of the intercalation of Li^+ ions during (**a**) discharge and (**b**) charging, demonstrating their rechargeable nature. (Inspired by S. Boparai et al. (2020) [17]).

For traditional binders, polyvinylidene fluoride (PVDF) is often used in LIBs [18]. However, issues arise with the organic solvent required for the slurry-processing in PVDF, N-methyl pyrrolidone (NMP), which is toxic, volatile, harmful to the environment and a hazard to workers' health [19]. Furthermore, PVDF too faces limitations as a binder for electrodes [20]. This mainly stems from its insulating nature and lack of flexibility, which in turn results in slow kinetics at high rates and a short usage lifetime when coupled with the swelling of electrodes during charging cycles [21,22]. The lack of flexibility in the binder can be especially detrimental to the cycling stability of the electrode, as any cracking that could occur would not be recoverable for brittle binders, leading to rapid battery degradation [23]. This is especially relevant for Si-based anodes, which will be discussed subsequently. As a result, there is a demand for exploration of other novel binders to address these limitations to further advance the electrochemical capabilities of LIBs.

2. Methodology

The articles for review and data collection for this research were carried out broadly following the PRISMA guidelines [24]. The journal articles referenced were sourced exclusively from Web of Science to ensure a manageable scope. The journal articles selected were restricted to those published in English within the last 5 years (published between 2020 and 2025; articles published in the first quarter of 2026 are also included in Section 4).

The search criteria for the various categories were that they must contain the category keyword (i.e., "Binder", "Slurry", "Manufacture") as well as containing the keywords "Lithium" or "Li" to ensure that the keywords applied to or were related to lithium battery

research only. For the binders category, subsequent filtering was done manually to include only articles that feature the investigation of utilizing alternative materials as binders within lithium-based batteries, while removing articles that focus on other aspects, such as investigation of their functions, synthesis and design principles, as well as those that are review articles on binders in lithium batteries. The remaining articles evaluating novel binders were categorized by title and abstract screening, then grouped by battery chemistry (e.g., Li-S, Li-ion) and binder characteristics (e.g., green binders, additives). The overall process is shown in Figure 4 below:

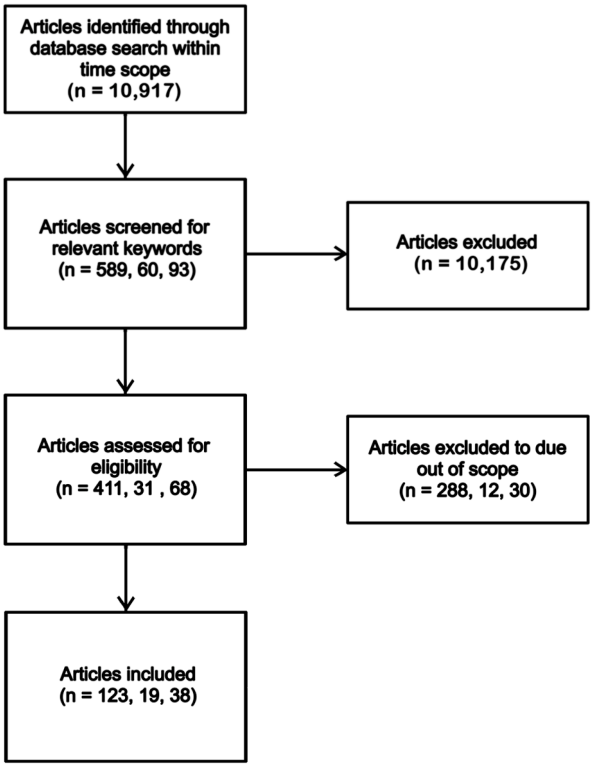

Figure 4. Diagram illustrating the PRISMA process for selection of assessed articles. Note that the three values of n are for the binder, slurry, and manufacture categories respectively.

From the categorized articles, the effect of the binder on the battery was mainly assessed through the comparison of the initial discharge capacity at the specified C rate, as well as the average rate of capacity loss (in %) of the battery per cycle at the specified C rate as reported in the literature. The capacity loss (in %) per cycle, if not already given in the articles, will be calculated by using a reported remaining capacity (either in %, Ag^{-1}, or Ahg^{-1}), the initial discharge capacity (in Ag^{-1}, or Ahg^{-1}) and the number of cycles at which the remaining capacity was taken.

In the case where the remaining capacity is given in %,

$$\text{Capacity loss (in \%)} = \frac{100 - R}{N}$$

In the case where the initial and remaining capacity is given in A g^{-1}, or Ah g^{-1},

$$\text{Capacity loss (in \%)} = \frac{I - R}{I \times N} \times 100\%$$

where R is the remaining capacity, I is the initial discharge capacity and N is the total number of cycles at which the remaining capacity was measured.

In cases where more than one testing condition and result was given, the most representative data given in the abstract and/or conclusion were taken as the representative data for the battery with that binder modification. For calculations of rate of capacity loss that are not directly given in articles, the average loss per cycle was calculated using the initial and final discharge capacity (or the final capacity retention in %) taking into account the number of cycles. For articles where units were given in A g^{-1}, the following formula was used to convert the testing conditions to C-rate [25]:

$$\text{C rate} = \frac{\text{Current density in mA g}^{-1}}{\text{Specific Capacity in mAh g}^{-1}}$$

A similar process was followed for the slurry and manufacturing categories, with the articles on slurry filtered to limit to only those that have a focus on optimization and alternative slurry synthesis, with novel methods, alternative additives and an assessment of environmental impacts, while the articles on manufacturing were filtered to limit to only those with a focus on alternative or optimized production methods, scalability and environmental impact assessments.

3. Results

In terms of the general amount of research done for each aspect of the battery that is considered in this review (namely: binders, slurry processes, manufacturing processes and framework, and recycling), an overall comparison between the years 2020–2026 (as of writing) was made based on articles available from Web of Science. The general numbers are obtained based on research that falls within each category, though not necessarily focusing on novel methods. The overall trend is shown in Figure 5 below (note that the data for 2026 are partial at the time of writing):

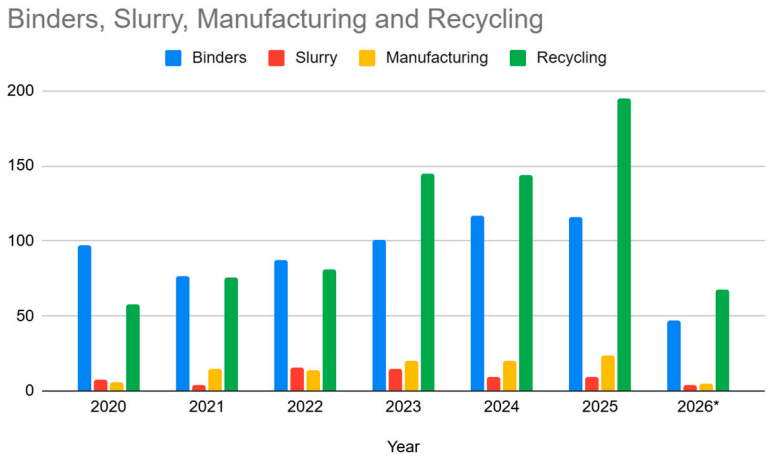

Figure 5. Trend of research progress for various categories over the years 2020–2026. * The data for 2026 are incomplete.

As observed, there is a general increase in the amount of research interest in the various aspects of Li-based batteries. The increase across the years is the most notable for research focusing on recycling, which increased from 58 articles in 2020 to 195 in 2025, suggesting much more focus on the environmental impacts and end-of-life processes of batteries in recent years.

Overall, 123 journal articles were assessed for alternative binder materials, 19 journal articles on alternative slurry processes, and 38 journal articles on alternative manufacturing processes and environmental assessments.

3.1. Alternative Binder Materials

3.1.1. Literature Survey Results

From the data collected using the methodology stated earlier, a total of 123 journal articles were recorded for research on binders of Li batteries between 2020 and 2025. It was noted that recent research progress for binder alternatives has been concentrated in three main categories: Li-S batteries, Li-ion batteries and other alternatives, with Li-S batteries accounting for 53 journal articles, Li-ion batteries accounting for 65 and alternative Li battery types (e.g., Li-Se, solid state, etc.) accounting for 5. The overall areas of research for battery binders are visualized in Figure 6.

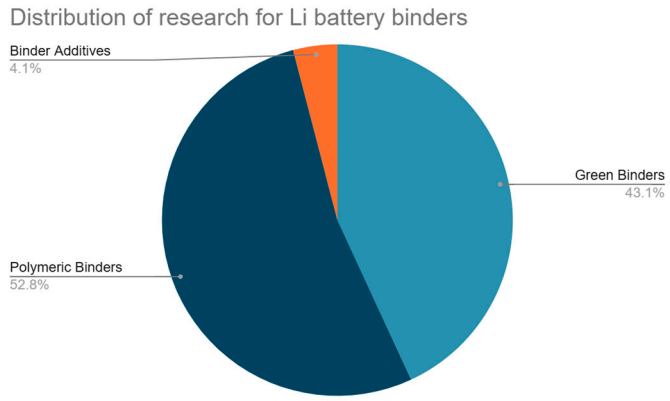

Figure 6. Distribution of research progress from journal articles reviewed under the Binder category.

Within the scope of each battery type, there is an intensifying research effort on the utilization of materials that are derivatives of natural substances (i.e., green binders) due to the increasing need for environmentally friendly alternatives to traditional binder materials such as PVDF. The utilization of various alternative polymers has also recently been explored, accounting for much of the research over the last 5 years (62.3% for Li-S and 72.3% for Li-ion batteries). The distributions of the research for the battery types are visualized in Figures 7 and 8.

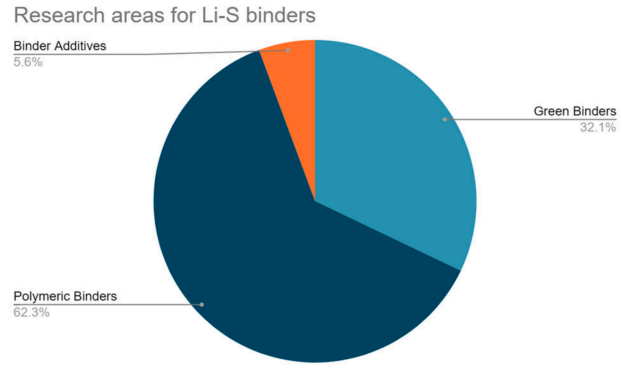

Figure 7. Distribution of binder research type within Li-S batteries.

3.1.2. Li-S Batteries

The major interest in lithium sulfur batteries is mainly due to the high theoretical specific capacity of sulfur electrodes (1675 mAh g^{-1}), low cost, and availability of sulfur in the Earth's crust [26], as well as the high energy density for a full cell ($\geq$600 Wh kg^{-1}) [27], demonstrating significant potential as an alternative to traditional lithium-ion battery compositions.

The traditional structure of a Li-S battery involves a positive electrode containing lithium and a negative electrode containing sulfur [17] (Figure 9).

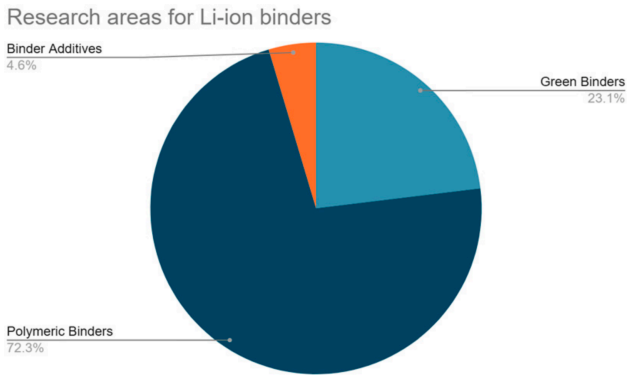

Figure 8. Distribution of binder research type within Li-ion batteries.

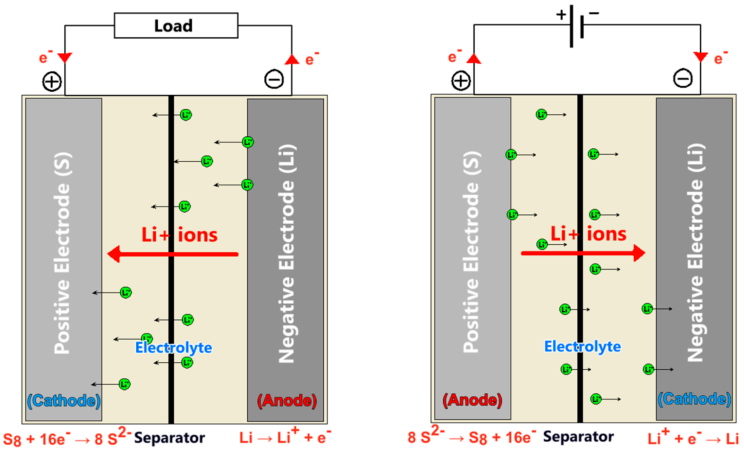

Figure 9. Diagram for reactions within Li-S battery during (**a**) discharge and (**b**) charging.

During charging, the lithium anode is oxidized to form lithium ions that can dissolve into the electrolyte and diffuse through the separator towards the cathode (same as Li-ion batteries) [17]. At the cathode, elemental sulfur would be reduced and would combine with the lithium ions to form lithium sulfides. The overall reaction for the charging cycle would be 16 Li + S_8 → 8 Li_2S, with Li_2S being the final product when the battery is fully discharged [28]. The reaction occurs in several steps, from elemental S_8 to S_8^{2-}, then S_6^{2-}, S_4^{2-}, and S_2^{2-}, before forming the eventual S^{2-} [29], leading to the formation of intermediate lithium polysulfides. During discharging, the reaction is reversed, with the Li_2S at the positive electrode being oxidized back into elemental S_8, releasing the Li ions that would diffuse back to the negative electrode and be reduced to Li metal [30].

The performance of the battery is often hindered by the shuttle effects of the lithium polysulfide active species, volume expansion of electrode and low reaction kinetics [31].

The shuttle effect refers to the back-and-forth movement of soluble polysulfide intermediates (Li_2S_X, $4 \leq x \leq 8$) between the electrodes of the battery during charge–discharge cycles, resulting in a loss of active species, corrosion of the anode, deterioration in capacity, and low Coulombic efficiency (Figure 10) [18].

The volume expansion is due to the formation of Li_2S from S_8 and their density differences, which leads to a significant volume change (≈80%) during the charging cycles [19,32], while the slow reaction kinetics are mainly due to the insulating nature of the active sulfur compounds [33].

Recent research on Li-S battery types can be classified into green binders, binder additives and alternative polymeric binders.

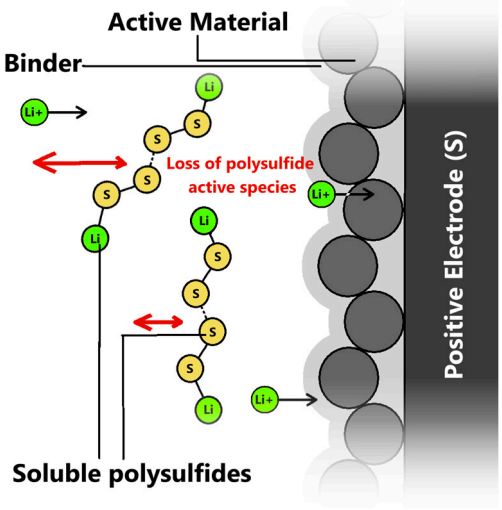

Figure 10. Diagram illustrating the shuttle effect of polysulfides in Li-S batteries.

Green binders refer to binder choices that have a focus on utilizing nature-based materials to address issues associated with Li-S battery systems. They may also have a focus on optimizing the production process of these batteries, as well as reducing the environmental impact resulting from the production, usage, or end-of-life processing of these batteries.

The data shown in Table 1 on the initial capacity for their respective C rate testing conditions that were available from the reviewed journals are plotted against each other in a scatter plot in Figure 11:

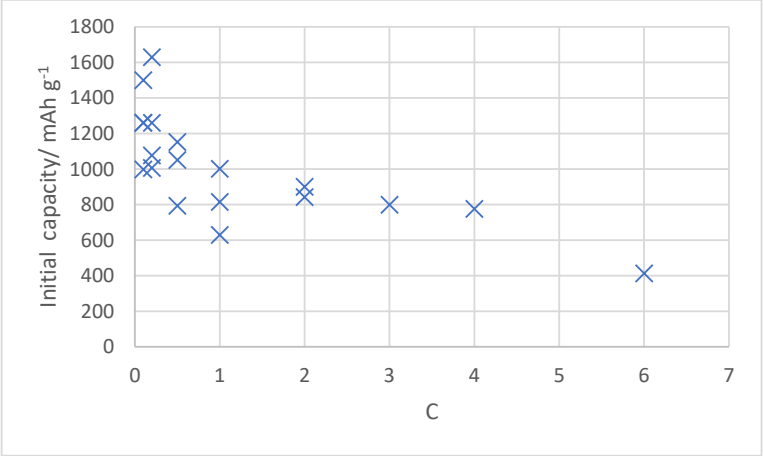

Figure 11. Plot of initial capacities against C testing conditions for the binders listed in Table 1 [31,34–48].

Several binders have been researched in Li-S batteries, but Carrageenan, a polysaccharide derivative of the Arctic red algae *Curdiea racovitzae* (CRP), seem to receive significant research attention. HY Jung et al. (2025) found that CRP is effective in preventing binder agglomeration and promotes the formation of a uniform 3D-structure, which facilitates the movement of electrolyte and utilization of sulfur species, which in turn likely contributes to the high initial capacity of 1500 mAh g^{-1} at 0.1 C (Table 1, Figure 4) that was reported [31]. This value is one of the highest reported for the green binders that were investigated, which implies its great potential for incorporation into future Li-S battery components. It was found that Carrageenan-based electrodes effectively trap short-chain lithium polysulfides and could chemically bind to active sulfur species. Considering its water-based process for the electrode

slurry preparation, Carrageenan hence has notable potential for scalability, environmental friendliness and cost-efficiency [37]. However, while good cycle stability and eco-friendly water-based preparation are observed, the strong binding properties of Carrageenan can also be a limitation as it could result in low porosity, which results in a lower capacity of the battery, as reported by Kazda T et al. (2021) [38] (578 mAh g^{-1} for S-Car-Iota electrode compared to 712 mAh g^{-1} for PVDF (Table 1)). Nonetheless, the strong retention of polysulfides in the Carrageenan binders makes it a promising candidate for natural binders.

Table 1. Data obtained for initial capacities and average capacity loss per cycle at various C rate conditions for the green binders (where available). (Note that, in addition to C rates, there are also other testing conditions, such as cycling voltage, that may differ across articles; hence, the comparisons are only approximate).

Binder Material	Initial Capacities/mAh g^{-1}	C Rate (for Capacities)	Capacity Loss per Cycle/%	C Rate (for Capacity Loss)	References
aloe vera gel (AG) with phytic acid (PA)	776.1	4	0.032	4	[34]
Boric Acid (BA) cross-linked to ramie gum (RG)	1001.6	1	0.027	4	[35]
Ramie gum (RG)	1152.2	0.5	0.088 *	0.5	[36]
Hybrid carrageenan	1500	0.1	-	-	[31]
	842	2	-	-	[31]
Carrageenan (CARR7)	1260	0.1	-	-	[37]
Carrageenan (CARR10)	997.9	0.1	0.039 *	4	[37]
Carrageenan (S-Car-Iota)	578	-	0.457 *	1	[38]
Carrageenan (S-Car-Lamb)	450	-	0.629 *	1	[38]
Lithium polysilicate (LSO) with tamarind polysaccharide gum (TPG)	1076.8	0.2	0.534 *	0.2	[39]
Peach Gum	793	0.5	0.047 *	0.5	[40]
Saccharide-based binder system (CMC glucose)	1629	0.2	-	-	[41]
cxNaPAA-XG/6.6Zn	815	1	0.018 *	1	[42]
	1006	0.2	0.113 *	0.2	[42]
Cationic waterborne polyurethane polymer with phytic acid (WPUP)	1051	0.5	0.066 *	0.5	[43]
phosphorylated soybean protein isolate (P-SPI), poly(ethylene oxide) (PEO) and phytic acid (PA) [SPP]	629.7	1	0.030	1	[44]
Doublecross-linked soy protein isolate (SPI)-polyacrylamide (PAM)	799.3	3	0.0992	3	[45]
	413	6	0.0545	6	[45]
Fenugreek gum	900	2	0.042 *	2	[46]
Methylated amino resin (MAR)	1261	0.1	0.253 *	0.1	[47]
N-Acetyl-L-Cysteine-Chitosan (NACCTS)	1260.1	0.2	0.018	2	[48]
Chloroprene rubber	-	-	0.210 *	0.05	[49]

* Values with [*] are calculated using data from the literature sources but not directly stated in the article.

Other commonly researched materials include various natural gums including Ramie [35,36], fenugreek [46], xanthan [42] and peach [40]. Among these binder materials, Ramie gum (RG) seems to be the most potential, with a high initial capacity of 1152.2 mAh g^{-1} (Table 1) [36]. The improvement in performance due to RG was attributed to the various oxygen- and nitrogen-containing functional groups of RG that impede the shuttle effects of the active sulfur species. Similar effects can be attributed to the enhanced binding and cycling stability for the incorporation of fenugreek gum in binders, where the formation of S-O and Li-O bonds in the functional groups reduces the mobility of polysulfide active species [46]. This is aligned with later findings for the binding mechanism in peach gum [40]. Metal ions can also be incorporated into the gum structures by triple cross-linking where the reactivity of zinc ions towards lithium polysulfides can be utilized to impede the shuttle effect of active sulfur species [42]. Similar strategy was used for a novel RB binder made using cross-linked Ramie gum and boric acid (BA), where the cross-linked structure was effective in improving flame retardancy and hence the usage safety of the Li-S batteries [35].

Using the data in Table 1 for capacity loss per cycle for the respective C rate testing conditions that were available from the reviewed journals, the results are plotted against each other in a scatter plot in Figure 12.

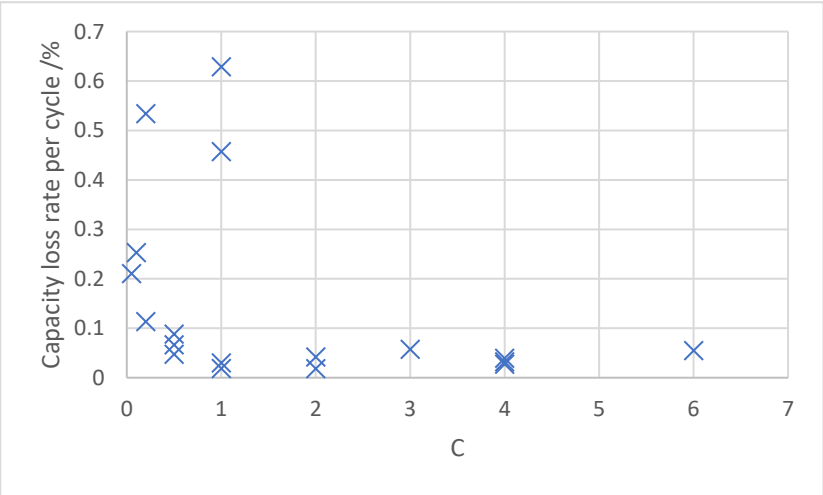

Figure 12. Plot of capacity loss per cycle against C testing conditions for the binders listed in Table 1 [34–40,42–49].

Most of the binder materials investigated by the articles have low capacity loss rates regardless of the C rate testing conditions, with the lowest capacity loss rates obtained using binders incorporating N-Acetyl-L-Cysteine-Chitosan (NACCTS), with a value of 0.018% loss per cycle (Table 2). The high retention of capacity was attributed to the enhancement of the transport kinetics of Li^+ ions by the polar groups of NACCTS, as well as the implementation of an adsorption redox-mediated synergism design. This design involves the amide group absorbing the lithium polysulfides, while the thiol group increases the redox kinetics of the reduction in polysulfides, which in turn leads to a reduction in the shuttle effect and hence a low rate of capacity loss [48]. A similarly low capacity-loss rate (0.018%) was calculated from the data for a triple cross-linked network containing xanthan gum, sodium poly(acrylic acid) and Zn^{2+} ions, where the reduction in the shuttle effect was attributed to the presence of Zn^{2+} ions that can interact with the polysulfides, though no increase in the redox kinetics was reported, unlike that for NACCTS [42]. Overall, many of the investigated binder materials follow similar principles in counteracting the shuttle effect of the Li-S battery, where various functional groups were used to trap the lithium

polysulfides, but few (like NACCTS) employ functional groups that also increase the redox kinetics of the reduction of the polysulfides into sulfide ions, which could contribute to the observation that NACCTS has better capacity retention compared to the other binder materials investigated. Hence, it would be useful to explore more multi-functional binders that serve both as a mitigator for shuttle effect as well as a facilitator for the reduction in polysulfide active species.

Table 2. Data obtained for initial capacities and average capacity loss per cycle at various C rate conditions for the binder additives. (Note that in addition to C rates, there are also other testing conditions, such as cycling voltage, that may differ across articles; hence, the comparisons are only approximate).

Binder Material	Initial Capacities/mAh g^{-1}	C Rate (for Capacities)	Capacity Loss per Cycle/%	C Rate (for Capacity Loss)	References
PVDF-g-(1-butyl-3-vinylimidazolium bis((trifluorompropyl)sulfonyl) imide)	792.5	0.5	0.11	0.5	[50]
Saponin	1410	0.05	0.012	2	[51]
	1200	0.2	-	-	[51]

Binder additives refer to materials that can be added in small amounts to traditional binder materials to enhance their properties.

For Li-S batteries, two articles on binder additives were collected, as shown in Table 2.

The data from Table 2 were plotted together with those obtained from the green binders for comparison in Figures 13 and 14.

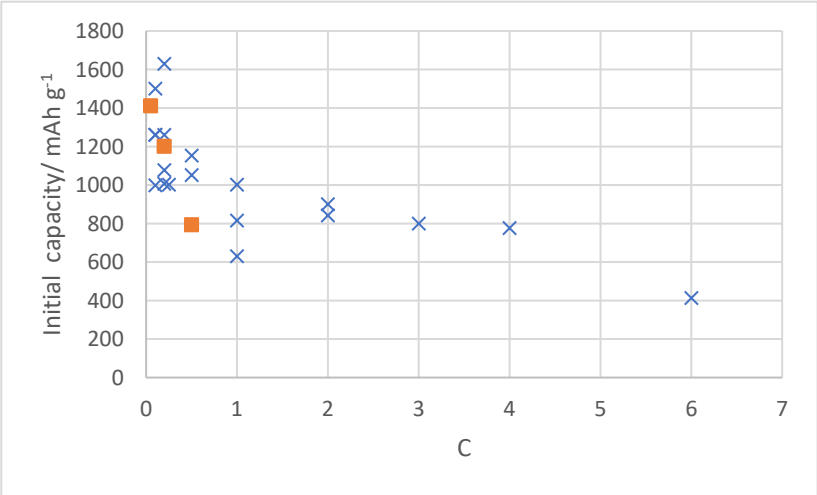

Figure 13. Plot of initial capacity against C testing conditions for binder additives (orange square) in comparison to green binders (blue cross), based on data from Table 2 [50,51].

From the data collected, it was noted that the performance of traditional binders with additive modifications is comparable to the novel green binders that were previously investigated, although the capacity seems to deteriorate faster as the C rate increases (but this observation has limited accuracy due to the very small sample size of data available).

The strategies employed in binder additives are similar to those in green binders, where additives provide functional groups for coordination to trap the polysulfides. For example, cationic monomer 1-butyl-3-vinylimidazole with bis(trifluoromethanesulfonyl)imide (TFSI–) was used as a binder additive by grafting it onto PVDF chains to coordinate with

lithium polysulfides. The presence of cationic polymer branches results in high binding energy between the binder and the polysulfide active material, leading to effective trapping of the polysulfides. Furthermore, the displacement of the TFSI-anion upon adsorption with lithium polysulfides also facilitates the movement of lithium ions into the cathode, hence improving the battery performance [50]. A similar result was obtained via the addition of saponin (1 wt.%), utilizing the hydroxyl groups present to link between the polysulfides and the traditional PAA binder, suppressing the shuttle effect and improving the cycling ability of the battery. Notably, saponin also serves as an effective dispersant in the synthesis process for the slurry due to its amphiphilic properties, hence improving the electrode coating quality [51]. As well as green binders and binder additives, various other polymeric binders were also investigated in recent years, as listed in Table 3.

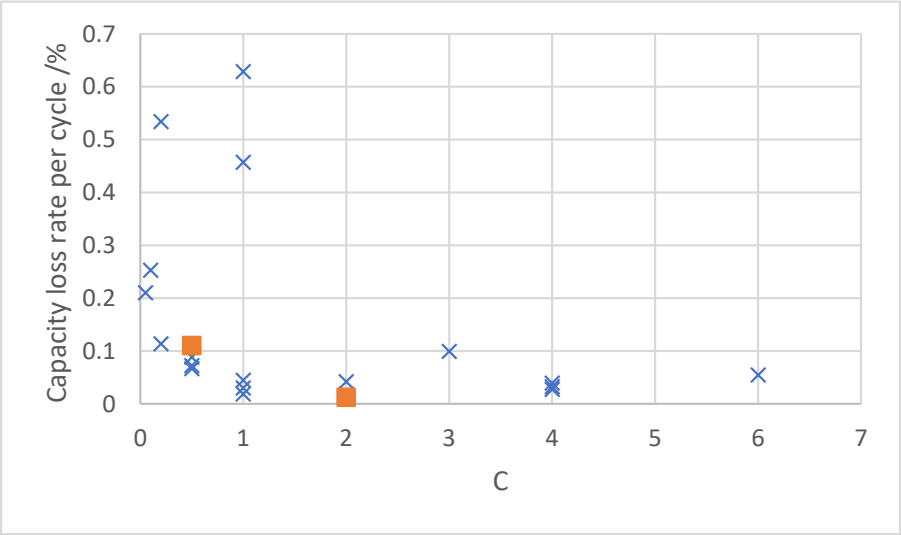

Figure 14. Plot of capacity loss per cycle against C testing conditions for binder additives (in orange) in comparison to green binders (in blue), based on data from Table 2 [50,51].

From Table 3, the data obtained were plotted together with the data points from binder additives and green binders in Figures 15 and 16.

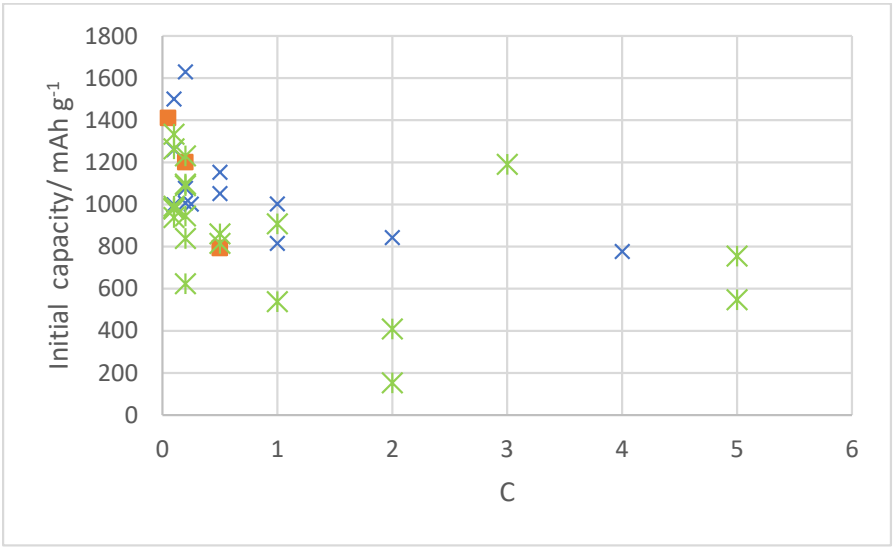

Figure 15. Plot of initial capacity against C testing conditions for other polymeric binders (green cross) in comparison to binder additives (orange square) and green binders (blue cross), based on data from Table 3 [52–81].

Table 3. Data obtained for initial capacities and average capacity loss per cycle at various C rate conditions for the other polymeric binders. (Note that in addition to C rates, there are also other testing conditions, such as cycling voltage, that may differ across articles; hence, the comparisons are only approximate).

Binder Material	Initial Capacities/mAh g^{-1}	C Rate (for Capacities)	Capacity Loss per Cycle/%	C Rate (for Capacity Loss)	References
3D cross-linked polyether binder (PTPO)	977.8	0.1	0.318 *	0.1	[52]
Ionically conductive elastic polymer (ICEP)	153	2	0.085 *	0.5	[53]
Polyvinyl alcohol-poly 2-acrylamido 2-methyl 1-propane sulfonic acid blend (PVA-PAAMPS)	815	0.5	0.056 *	0.5	[54]
	1264	0.1	0.110 *	0.1	[54]
lipoic acid and zwitterionic monomer 2-methacryloyloxyethyl phosphorylcholine (PLM)	1096.3	0.2	0.041	1	[55]
lipoic acid, polyethylene glycol diacrylate, 2-methacryloyloxyethyl phosphorylcholine LA-PEGDA-MPC (LPM)	907.4	1	0.039	1	[56]
PAA-PVA-BA (PPB)	408.1	2	0.078 *	0.5	[57]
Poly(ether-thioureas) (PETU) and poly(3,4-ethylenedioxythiophene)-poly(styrenesulfonate) (PEDOT:PSS)	754.3	5	0.140 *	0.5	[58]
cationic imidazole group on polymethyl methacrylate (PMMA) backbone (PIL)	547.3	5	0.062	2	[59]
polymeric aluminophosphate (AP)	1190	3	0.002	3	[60]
hexamethylolmelamine on polyacrylic acid (HMM/PAA)	838.2	0.2	0.182	1	[61]
lipoic acid-gallic acid (LA-GA)	1088.7	0.2	0.047	1	[62]
			0.181 *	0.2	[62]
beta-CDp-Cg-2AD	1333	0.1	0.040 *	0.1	[63]
polyvinyl alcohol (PVA) and tartaric acid (TA).	537.7	1	0.140	1	[64]
Al-coordinated polyethyleneimine (PEI-Al)	938	0.1	0.130 *	0.1	[65]
polyacrylamide, locust bean gum and gellan gum (PLG)	623.4	0.2	0.257 *	0.2	[66]
gamma-polyglutamic acid (gamma-PGA)	991	0.1	0.375 *	0.2	[67]
zwitterionic sulfobetaine methacrylate (SBMA), poly(ethylene glycol) methyl ether acrylate (PEGA), and 2-hydroxyethyl acrylate (HEA) (ZIP)	1230.6	0.2	0.030	2	[68]

Table 3. *Cont.*

Binder Material	Initial Capacities/mAh g^{-1}	C Rate (for Capacities)	Capacity Loss per Cycle/%	C Rate (for Capacity Loss)	References
polyethyleneimine (PEI), polyvinylpyrrolidone (PVP), citric acid (CA), and polyethylene oxide (PEO) (PPCP)	981.6	0.1	0.028	1	[69]
Amphoteric Polymer (CPAM&HBPE)	860	0.5	0.056	2	[70]
cross-linked quaternary ammonium cationic starch (c-QACS)	944.8	0.2	0.307	0.5	[71]
cross-linked chitosan sulfate network (CCSN)	824	1	0.051 *	4	[72]
			0.082	1	[72]
poly(ethylene oxide)-b-poly(4-vinyl catechol) (PEO-b-P4VC)	1115	0.5	0.053 *	0.5	[73]
Poly(vinyl pyrrolidone) (PVP) and carboxylated nitrile butadiene rubber (XNBR)	1018	0.2	0.020	1	[74]
Polyacrylic acid (PAA) cross-linked by cationic hydroxypropyl polyrotaxane (HPRN+)	1000.9	0.25	0.045	1	[75]
hyperbranched poly(amidoamine) (HPAA)	601	0.2	0.040	0.1	[76]
ring-opened poly(vinylpyrrolidone) (PVP) connected with reduced graphene oxide (rGO)	964	0.2	0.252 *	0.2	[77]
ionic cross-linked polymer (DICP)	1035	0.5	0.496 *	0.5	[78]
An amine group containing benzo(ghi)perylene imide (BPI) grafted onto poly(acrylic acid)	800	0.5	0.036	0.5	[79]
poly[2,2′-(2,2″,4,4″,6,6″-hexamethyl-p-terphenyl-3,3″-diyl)-5,5′-bibenzimidazolium iodide] (HMT-PMBI(I-))	1037	0.1	0.059	0.5	[80]
Chitosan-rGO Network	1019	0.2	0.016	1	[81]

* Values with [*] are calculated using data from the literature sources but not directly stated in the article.

Comparing the initial capacities, it is noted that the capacity of other polymeric binders is slightly lower overall than that of green binders, though this may be attributed to the much smaller sample size of the green binders relative to other polymeric binders. However, the general rate of capacity loss for other polymeric binders is seen to be less than in those with more focus on the incorporation of natural materials.

In recent years, significant research attention has been directed toward the structural modification of polyacrylic acid (PAA) to enhance its physicochemical and electrochemical performance. The popularity of PAA as an alternative binder base can be attributed to its solubility in water, making it a more environmentally friendly option compared to the PVDF and NMP solvents used for synthesis [57,61,75]. Efforts to improve performance are largely motivated by the need to develop multifunctional polymer binders with improved

mechanical integrity, thermal stability, and interfacial activity. Broadly, modification strategies have centered on copolymerization, cross-linking, and molecular grafting, enabling the systematic tuning of PAA's architecture and functionality. Cross-linking approaches have been particularly effective in reinforcing the polymer network and improving stability. For example, PAA-based copolymers cross-linked with poly (vinyl alcohol) (PVA) and boric acid (BA) could lead to the formation of a three-dimensional network that could impart enhanced thermal stability [57]. Similarly, cross-linking PAA with hexamethylolmelamine (HMM) yields a mechanically robust binder with improved adhesive strength. Importantly, beyond mechanical enhancement, the HMM/PAA system exhibits accelerated redox kinetics, which is linked to favorable chemical interactions between the binder and lithium polysulfide species [61]. Cross-linking PAA with cationic hydroxypropyl polyrotaxane (HPRN+) also results in enhanced adhesive strength and elastic modulus, hence providing effective mitigation to the volume fluctuations in the electrodes during charging cycles, and in turn improving the cycling capabilities and capacity retention of the battery [75].

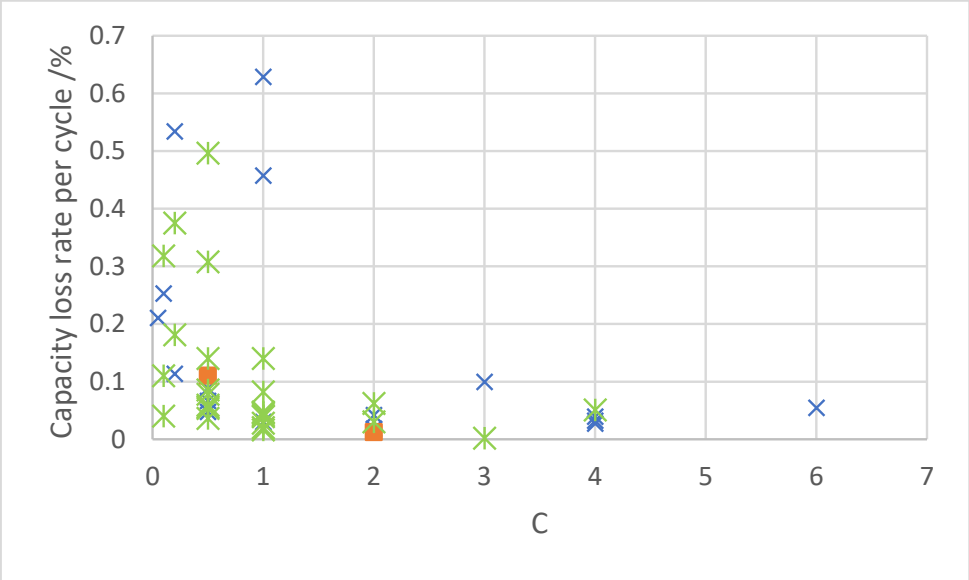

Figure 16. Plot of capacity loss per cycle against C testing conditions for other polymeric binders (green cross) in comparison to binder additives (orange square) and green binders (blue cross), based on data from Table 3 [52–81].

In addition to cross-linking, the grafting method has also been explored, particularly through the addition of benzo(ghi)perylene imide (BPI) onto a PAA base. Notably, BPI can act as a redox-mediating reagent to improve the redox kinetics of the lithium polysulfides, facilitating the reduction from polysulfides to Li_2S [79]. This strategy is similar to other binders mentioned earlier, such as the use of NACCTS [48] and the HMM/PAA system [61].

Zwitterionic polymer binders have emerged as a promising class of materials due to their ability to simultaneously enhance electrochemical performance and mechanical stability. These systems often rely on dynamic non-covalent cross-linking, enabling ion–dipole interactions with active species that facilitate improved redox kinetics while accommodating volume changes during charge–discharge cycling. The capacity value of 1333 mAh g^{-1} has been reported for a binder containing β-cyclodextrin polymer (β-CDp) as a host with choline glycerophosphate (Cg) and a supramolecular cross-linking agent (2AD) as the guests, which was the highest among the binders investigated in this category [63]. In contrast to conventional polar binders, this interaction mechanism provides greater structural adaptability and stress tolerance [68]. Additionally, the presence of hydrogen bonding and electrostatic interactions imparts self-healing properties, which help mitigate

electrode cracking and improve long-term cycling stability. Functional groups such as phosphate and carboxylate further contribute to enhanced electrochemical activity [55]. Combined with their inherent water-solubility, these characteristics position zwitterionic binders as strong candidates for high-performance and environmentally sustainable battery systems [63,68].

As a conclusion, from the assessment of various alterative binder designs, the incorporation of various polar groups, which was shown to be achieved via grafting [50,61,79] or the establishment of a functional group [48,51], into the binder design allows for stronger trapping interactions between these functional groups and the polysulfide active species and works to reduce the loss of these species via the shuttle effect that is prevalent in Li-S batteries. In turn, the reduction in shuttle effect serves to extend the usage lifetime of the battery, as it slows down the rate of degradation over charge–discharge cycles. Charged species within the binders seem to be particularly effective due to their stronger ion–dipole interactions as well as through facilitating Li^+ transport through these interactions [48], as shown in the use of Zn^{2+}, TFSI- and various zwitterions [42,50,55]. Furthermore, amide groups are shown to be particularly effective in enhancing the redox kinetics of the active species, due to the ability to act as sulfophilic active sites and form amide–thiol–amide structures that follow the three-dimensional instantaneous nucleation model (3DI) model and result in rapid nucleation at the electrode [48].

Attempts to improve the mechanical integrity of electrodes mainly consider the resilience of the material to volumetric expansion under cycling conditions (i.e., through imparting self-healing properties). Zwitterions again are particularly effective due to the presence of oppositely charged groups and the ability to establish electrostatic interactions with each other [55], which in turn allow the binder to encase the electrode and counteract the extent of expansion during charging cycles, improving cycle stability.

From an environmental perspective, end-of-life processing would benefit from a reduction in disposed batteries as their cycling stability increases and their rate of degradation decreases, allowing for a longer duration of use for each individual battery.

3.1.3. Li-Ion Batteries

Lithium-ion batteries often utilize lithium metal (without binder) or graphite as the anode [16]. However, these often face challenges such as dendritic growth (especially lithium metal) that could reduce cycling efficiency and result in severe safety concerns [82] (due to the dendrites potentially piercing the separator and resulting in an internal short-circuit [16]), as well as shortening the operational lifespan of the battery [83]. Common choices of cathodes such as alloy materials would face issues such as large volume expansions that could result in material cracking and structural damage, leading to battery degradation [15].

In recent years, silicon-based anodes have also become a promising alternative due to their high theoretical capacity and low operating potential, as well as their abundance and non-toxicity [84,85]. During lithiation (charging), amorphous phases (Li_xSi with x = 0–3.75) form first and will subsequently transform into $Li_{15}Si_4$. During de-lithiation (discharging) the crystalline $Li_{15}Si_4$ phase transforms back to amorphous Si [86,87]. However, it too faces issues of volumetric fluctuation during charging cycles, unstable interfaces and poor conductivity due to alloying/dealloying processes, leading to poor cycling performance [84,88].

The data obtained from Table 4 is plotted as a scatter plot in Figure 17:

Table 4. Data obtained for initial capacities at various C rate conditions for the green binders, together with their anode system. (Note in addition to C rates, other tests may differ across articles; hence, the comparisons are only approximate).

Binder Material	Anode System Used	Initial Capacities/mAh g^{-1}	C Rate	C Rate in mA g^{-1}	References
Cellulose levulinate ester (CLE)	Li-foil	100	6	-	[89]
Cellulose nanofiber (TOCNF)	-	163	0.1	-	[90]
hydroxybutyrate, with 47% 4-hydroxybutyric acid	C (Graphite)	302	0.0662 *	20	[91]
Starch, PVA, sodium tetraborate (Si@SPS)	Si	2420	0.413 *	1000	[92]
Si @ fibrin (with alginate)	Si	1210	0.5	-	[93]
guar gum (GG) and carboxylated acrylonitrile-butadiene rubber (XNBR)	Si/C	149	0.5	-	[94]
Si@X4G6	Si	2615	0.153 *	400	[94]
sodium alginate (E-SA)	C	164.7	0.1	-	[95]
Borax between strands of polyacrylic acid (PAA) Si-PAA-5B	Si	2470	0.202 *	500	[96]
Tapioca starch binder modified with polyethylene glycol (PEG)	Si	3486	0.0574 *	200	[97]
Binder with the dissolved spider silk (SWS) cells	Si-based	3642	0.0686	250	[98]
Si nanoparticles (SiNPs) encapsulated in Citric Acid (CA)	Si-Graphite oxide	3266	0.306 *	1000	[99]
Tamarind Kernel Powder (TKP)	C (graphite)	426	0.1	-	[100]
Pectin	Si-based	3175	0.1	-	[101]
natural sesbania gum (SG)	Si-based	2023	0.494 *	1000	[102]
White Latex	C (graphite)	357	0.1	-	[103]

* Values with [*] are calculated using data from the literature sources but not directly stated in the article.

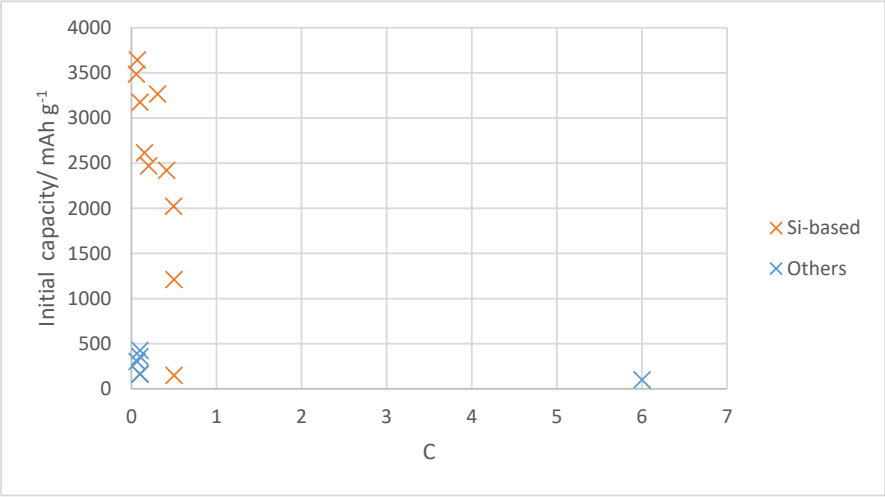

Figure 17. Plot of initial capacity against C testing conditions for green binders listed in Table 4 [89–103].

Among the binders investigated for Li-ion batteries, green binders for systems utilizing Si anodes are seen to yield significantly higher initial discharge rates compared to systems utilizing other anode materials such as lithium foil and graphite. This is expected due to

the much higher theoretical capacity of Si-based LIBs (~4200 mAh g^{-1}) [104] compared to graphite-based LIBs (~372 mAh g^{-1}) [105]. Nonetheless, a relatively large range of capacity values was observed for green binders for Si-based LIBs compared to graphite-based LIBs, suggesting that the choice of binders have larger possible impacts on the performance of Si anodes (Figure 17).

Among the green binders of Si-based LIBs investigated, much has been explored regarding the incorporation of natural materials into binder designs in recent years. Notably, derivatives of spider silk were incorporated into binders (SWS) to mitigate the issue of volume expansion in Si anodes during charging cycles. The highest discharge capacity value of 3642 mAh g^{-1} was reported for the first cycle, together with a much longer retention of capacity relative to the Si-PVDF control cell, demonstrating the effectiveness of the SWS binder in promoting cycling stability. The design took advantage of the unique crystal structures, superior adhesion, close-packing of protein blocks and the side chain R-group of crystal β-sheet of spider silk to enhance the performance of the binder, displaying the advantages of using natural materials to enhance binder properties [98].

Similar to green binders for Li-S batteries, the use of natural plant-based gums seems to have gathered much research interest recently, as is evident from the investigation of guar, pectin and sesbania gum. These natural derivatives have numerous functional groups, such as carboxylic acids, enhancing interactions between the anode and the binder and hence mitigating the effects of volume expansion. Notably, gums like pectin are commonly found in peels and seeds, and hence can be extracted from common food industrial wastes and provide an especially low-cost and eco-friendly alternative [101]. Moreover, guar gum (GG) was found to have self-healing properties when coupled with carboxylated acrylonitrile-butadiene rubber (XNBR), further enhancing the cycling stability of Si LIBs [94].

Among the green binders utilized in graphite and Li foil LIBs, the highest initial discharge capacity of 426 mAh g^{-1} was achieved with the use of Tamarind Kernel Powder (TKP) as an aqueous binder on graphite anodes, significantly surpassing the capacities for traditional graphite anodes. The enhanced performance of the electrode was attributed to low swelling of the binder and its branched structure, consisting of hydroxyl functional groups that are capable of bonding interactions. Together with its non-toxicity, ease of handling and low processing cost, it is an attractive binder option for graphite anodes and is proposed to be effective on other electrode materials, as well as other Li-based battery systems (e.g., Li-S) [100].

The data obtained from Table 5 are plotted as a scatter plot in Figure 18:

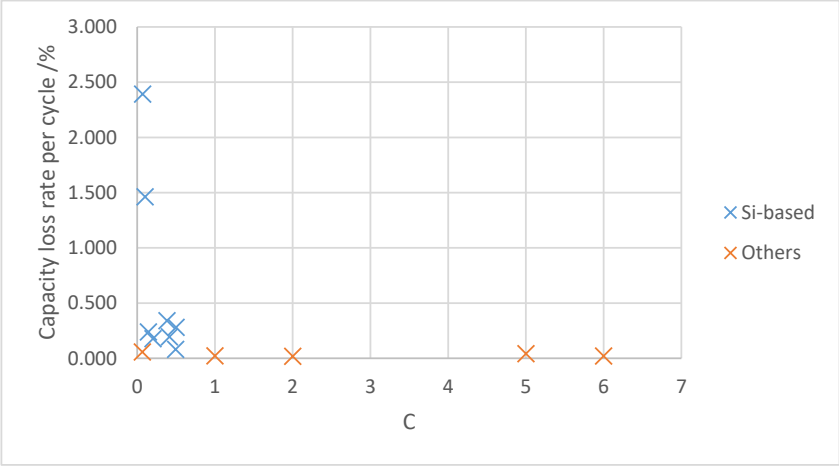

Figure 18. Plot of capacity loss per cycle against C testing conditions for green binders listed in Table 5 [89–94,96–103].

Table 5. Data obtained for capacity loss per cycle at various C rate conditions for green binders, together with their anode system. (Note that in addition to C rates, there are also other testing conditions, such as cycling voltage, that may differ across articles; hence, the comparisons are only approximate).

Binder Material	Anode System Used	Capacity Loss per Cycle/%	C Rate	C Rate in mA g^{-1}	References
CLE	Li-foil	0.020 *	6	-	[89]
CTOCNF	-	0.040 *	5	-	[90]
hydroxybutyrate, with 47% 4-hydroxybutyric acid	C (Graphite)	0.056 *	0.0662 *	20	[91]
Starch, PVA, sodium tetraborate (Si@SPS)	Si	0.194 *	0.413 *	1000	[92]
Si @ fibrin (with alginate)	Si	0.280 *	0.5	-	[93]
GG-XNBR	Si/C	0.340 *	0.382 *	1000	[94]
Borax between strands of polyacrylic acid (PAA) Si-PAA-5B	Si	0.176 *	0.202 *	500	[96]
Tapioca starch binder modified with PEG	Si	0.238 *	0.143 *	500	[97]
Binder with the dissolved spider silk (SWS) cells	Si-based	2.391 *	0.0686	250	[98]
Si nanoparticles (SiNPs) encapsulated in CA	Si-Graphite oxide	0.214 *	0.306 *	1000	[99]
TKP	C (graphite)	0.195 *	0.1	-	[100]
Pectin	Si-based	1.46 *	0.1	-	[101]
SG	Si-based	0.08 *	0.494 *	1000	[102]
White Latex	C (graphite)	0.035 *	0.3	-	[103]

* Values with [*] are calculated using data from the literature sources but not directly stated in the article.

Comparing the cycling performance of the Si-based, graphite-based and other LIB binders assessed, Si-based LIB binders showed significantly higher loss of capacity per cycle relative to other LIBs, which can be attributed to the possibly larger volume fluctuations of Si-based anodes compared to other types due the alloying/dealloying processes that occur rather than the intercalation processes that occur in graphite anodes.

Among the Si-based anodes, the lowest calculated rate of capacity loss, with a value of 0.08%, was achieved using sesbania gum (SG) on silicon nanoparticles. This low capacity loss was attributed to the strong mechanical properties of SG binders, which can resist the volume changes in the silicon during charging cycles, making the modulus and hardness of the binder an important factor contributing to its performance in cycling tests [102].

For graphite-based anodes, the use of white latex was the most effective in reducing capacity loss rate, with a calculated value of 0.035%. This low rate of capacity loss was attributed to the strong adhesion properties and low electrolyte swelling of the binder, together with the high surface coverage and collaboration with the anode, resulting in enhanced performance and offering a better alternative to traditional PVDF binders [103].

In addition, four articles on additives were investigated, with their performance listed in Tables 6 and 7.

Various additives to binders for Si- and graphite-based LIBs were also explored in recent years, showing similar improvements in electrochemical performances between Si- and graphite anodes with various binders.

Table 6. Data obtained for initial capacities at various C rate conditions for binder additives, together with their anode system. (Note that in addition to C rates, other tests may differ across articles; hence, the comparisons are only approximate).

Binder Material	Anode System Used	Initial Capacities/mAh g^{-1}	C Rate	References
Trisiloxane-based additive	Graphite, 15 wt.% SiO	647	2	[106]
PEDOT:PSSTFSI	C	140	0.1	[107]
PPCPTMC and PE-PEO	Graphite	-	-	[108]
Citric acid and oxidized graphene modified by p-aminobenzenesulfonic acid	Si	1590	0.629 * (0.1A g^{-1})	[109]

* Values with [*] are calculated using data from the literature sources but not directly stated in the article.

Table 7. Data obtained for capacity loss per cycle at various C rate conditions for binder additives, together with their anode system. (Note that in addition to C rates, there are also other testing conditions, such as cycling voltage, that may differ across articles; hence, the comparisons are only approximate).

Binder Material	Anode System Used	Capacity Loss per Cycle/%	C Rate	References
Trisiloxane-based additive	Graphite, 15 wt.% Si-O	0.075 *	0.2	[106]
PEDOT:PSSTFSI	C	0.171 *	0.2	[107]
PPCPTMC and PE-PEO	Graphite	-	-	[108]
Citric acid and oxidized graphene modified by p-aminobenzenesulfonic acid	Si	0.090 *	0.629 * (0.1A g^{-1})	[109]

* Values with [*] are calculated using data from the literature sources but not directly stated in the article.

Notably, the strong adhesion provided by p-aminobenzenesulfonic acid modifications on graphite-oxide and Si nanoparticles with citric acid was effective in preventing slipping between Si nanoparticles as a result of volume expansion, improving the mechanical stability and hence leading to a superior cycling performance [109]. Furthermore, additives to PVDF can be incorporated via copolymerization, enhancing the dispersion of active materials in the electrodes and increasing electrochemical performance. However, it was noted that excessive amounts of additives such as PPC-PTMC and PE-PEO could lead to faster cell deterioration [108].

Nonetheless, some polymeric binders can also be multifunctional, playing the role of conductive additives as well. PEDOT:PSSTFSI was shown to be effective in replacing both PVDF and carbon black in LIBs, achieving higher reversible capacities and enhancing capacity retention. Furthermore, the removal of other additives, such as carbon black, reduces the reactivities at interfaces, increasing the stability of these interfaces as a result [107]. In addition, cross-linking can also be used to incorporate additives, with trisiloxane acting as an effective dispersion agent as well as enhancing the wettability of electrolyte through the process of in situ cross-linking during fabrication. Furthermore, such additives can be applied to various electrodes that face issues of volume expansion, though attention to the exact ratios of additives is needed such that sufficient functional groups are retained for hydrogen bonding to the electrode [106].

Various other polymeric binders were also explored, with their electrochemical performance listed in Tables 8 and 9, and the data visualized in Figures 19 and 20.

Table 8. Data obtained for initial capacities at various C rate conditions for other polymeric binders. (Note that in addition to C rates, other tests may differ across articles; hence, the comparisons are only approximate).

Binder Material	Binder Type	Initial Capacities/mAh g^{-1}	C Rate	C Rate in mA g^{-1}	References
acrylic acid and hydroxyethyl acrylate (AA-HEA),(XNBR)	Anode	465.2	0.5	-	[110]
	Anode	466.51	2	-	[110]
Polyetherurea with Styrene–Butadiene Rubber (SBR)	Cathode	148	0.06	-	[111]
Sulfobetaine methacrylate and poly(ethylene glycol) methyl ether methacrylate zwitterionic polymers (ZIPs)	Cathode	111.2	3	-	[112]
Se-Se bonds containing polyurethanes (PUPEG-2000)	Cathode	139.77	1	-	[113]
Polyspirobifluorene-based binder (PSFB)	Cathode	370	0.05	-	[114]
Cross-linked PVA/malonic acid (MA)	Anode	593	0.5	-	[115]
Poly (propylene carbonate) (PPC)	Cathode	112.2	1	-	[116]
Rigid PAA and flexible polylipoic acid (PTA)	Anode	884.8	0.5	-	[117]
Poly(oxycarbonylmethylene 1-allyl-3-methyimidazolium) (PMAI)	Anode	297	1	-	[118]
Sodium carboxymethyl cellulose (CMC-Na) and waterborne polyurethane (WPU)	Anode	2626.2	0.1	-	[119]
Polyurethane (PU)	Cathode	373	0.1	-	[120]
Cross-linked MDI-based waterborne polyurethane (TMPU)	Anode	1462.16	0.137 *	1000	[121]
Poly (propylene carbonate)-plus (PPC-P)	Cathode	160	0.5	-	[122]
taurine-grafted-poly (acrylic acid) binder (Tau-g-PAA)	Anode	1003	1	-	[123]
BDSA-DPA-PEGCE	Anode	2567	0.390 *	1000	[124]
TA-PEDOT:PSS (TAPE)	Cathode	95	10	-	[125]
Alginate, PEO and PVP (2:1:1)	Anode	165	1	-	[126]
thiourea polymer network (TUPN10)	Anode	2087.7	0.479 *	1000	[127]
poly(propylene carbonate) (PPC)	Cathode	141.9	0.5	-	[128]
polyimide-based aromatic polymer (PAID20)	Anode	2663	0.2	-	[129]
poly(methyl methacrylate)grafted natural rubber (MG49) [G6 –10]	Anode	265.3	0.1	-	[130]
poly(methyl methacrylate)grafted natural rubber (MG49) [G6 –15]	Anode	299.8	0.1	-	[130]
poly(2,2′-disulfonyl-4,4′-benzidine terephthalamide) (PBDT)	Anode	1010.5	0.2	-	[131]
polymer gel binder consisting of chitosan, the ionic liquid PYR14 DCA, and the lithium salt (LiTFSI) (PGB)	Anode	583	0.5	-	[132]
cross-linked sodium polyacrylate [CLPA-20]	Anode	1650	0.0606 *	100	[133]
cross-linked poly(N-allyl-vinyl imidazolium) (C-PAVIm)	Anode	610	0.05	-	[134]
polyrotaxane -TFMSI-Li (SSIP)	Anode	1650	0.5	-	[135]
PDADMA-CFSO	Cathode	125	0.3	-	[136]

Table 8. *Cont.*

Binder Material	Binder Type	Initial Capacities/mAh g^{-1}	C Rate	C Rate in mA g^{-1}	References
PDADMA-FSI	Cathode	123	0.3	-	[136]
PDADMA-BETI	Cathode	116	0.3	-	[136]
PDADMA-TFSI	Cathode	114	0.3	-	[136]
Sulfated Alginate SO3-ALG	Cathode	140	0.143 *	20	[137]
beta-cyclodextrin polymer (beta-CDp)	Anode	3869	0.0517 *	200	[138]
3% PBDT-LFP	Anode	160	0.2	-	[139]
P-BIAN/PAA	Anode	3202	0.156 *	500	[140]
	Anode	2100	0.238 *	500	[140]
acrylic acid and glyceryl (7%)	Anode	1170	0.427 *	500	[141]
poly(ether-thioureas) (TUEG) on PAA	Anode	3676.1	0.05	-	[142]
dopamine-modified CMC	Anode	3418	0.293 *	1000	[143]
P-HAEAPMA	Anode	648.2	0.2	-	[144]
PAA-FREP	Anode	3450	0.0290 *	100	[145]
PGB	Both	244	10	-	[146]
PProDOT-Hx(2)	Anode	168	0.2	-	[147]
carboxymethyl cellulose and polydopamine	Anode	2303	0.2	-	[148]
Pd(PPh3)(4) catalys, dibromo benzoic acid, dioctylfluorene-diboronic acid bis(1,3-propanediol) ester.	Anode	2036	0.333	-	[149]
polyimine	Anode	804.4	2.49 *	2000	[150]
	Anode	2114	0.189 *	400	[150]
	Anode	1087.8	1.84 *	2000	[150]
bPAA-3	Anode	752	0.5	-	[151]
palladium-catalyzed direct arylation of 3-(2-ethylh exhyl) thiophene or 3,3′-di(2-ethylhexyl)bithiophene and dimethyl-2,5-dibromoterephthalate, followed by saponification.	Anode	2700	1	-	[152]

* Values with [*] are calculated using data from the literature sources but not directly stated in the article.

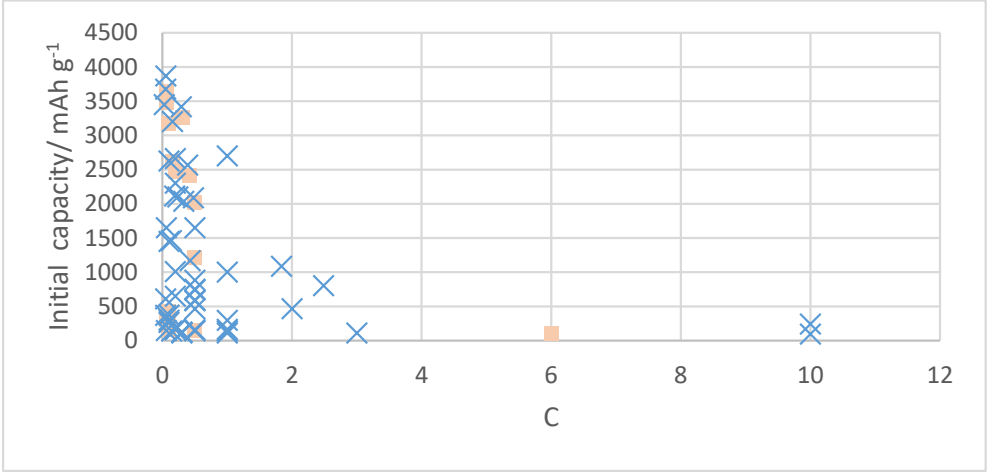

Figure 19. Plot of initial capacity against C testing conditions for other polymeric binders (blue cross) in comparison with green binders (light orange square), based on data from Table 8 [110–152].

Table 9. Data obtained for capacity loss per cycle at various C rate conditions for other polymeric binders. (Note that in addition to C rates, there are also other testing conditions, such as cycling voltage, that may differ across articles; hence, the comparisons are only approximate).

Binder Material	Binder Tye	Capacity Loss per Cycle/%	C Rate	C Rate in mA g^{-1}	References
Polyetherurea with SBR	Cathode	0.022 *	0.06	-	[111]
ZIPs	Cathode	0.0132 *	3	-	[112]
Se-Se bonds containing polyurethanes (PUPEG-2000)	Cathode	0.0553 *	1	-	[113]
PSFB	Cathode	0.0784 *	0.1	-	[114]
Cross-linked PVA/MA	Anode	0.0925 *	0.5	-	[115]
PPC	Cathode	0.1195 *	1	-	[116]
Rigid PAA and flexible PTA	Anode	0.225 *	1	-	[117]
PMAI	Anode	0.0267 *	1	-	[118]
CMC-Na and WPU	Anode	0.08	0.1	-	[119]
PU	Cathode	0.141 *	0.1	-	[120]
TMPU		0.2578 *	0.684 *	1000	[121]
PPC-P	Cathode	0.0314 *	1	-	[122]
taurine-grafted-poly (acrylic acid) binder (Tau-g-PAA)	Anode	0.1658 *	0.2	-	[123]
BDSA-DPA-PEGCE	Anode	0.566 *	0.390 *	1000	[124]
TA-PEDOT:PSS (TAPE)	Cathode	0.0164 *	1	-	[125]
Alginate, PEO and PVP (2:1:1)	Anode	0.0116 *	0.33	-	[126]
thiourea polymer network (TUPN10)	Anode	0.267 *	0.479 *	1000	[127]
PPC	Cathode	0.0261 *	0.5	-	[128]
MG49 [G6-10]	Anode	0.306 *	0.1	-	[130]
MG49 [G6-15]	Anode	0.444 *	0.1	-	[130]
PBDT	Anode	0.18 *	0.2	-	[131]
PGB	Anode	0.0609 *	0.5	-	[132]
cross-linked sodium polyacrylate [CLPA-20]	Anode	0.141 *	-	-	[133]
C-PAVIm	Anode	0.689 *	-	-	[134]
polyrotaxane-TFMSI-Li (SSIP)	Anode	0.02 *	0.5	-	[135]
	Anode	0.25 *	0.033	-	[135]
(PAA-g-SBR), 80% Na-PAA	Anode	0.0113 *	-	-	[153]
PDADMA-CFSO	Cathode	0.018 *	3	-	[136]
PDADMA-BETI	Cathode	0.024 *	3	-	[136]
beta-CDp	Anode	0.289 *	0.0517 *	200	[138]
3% PBDT-LFP	Anode	0.005 *	4	-	[139]
P-BIAN/PAA	Anode	0.00833 *	0.238 *	500	[140]
acrylic acid and glyceryl (7%)	Anode	0.46 *	0.427 *	500	[141]
TUEG on PAA	Anode	0.06 *	0.5	-	[142]

Table 9. *Cont.*

Binder Material	Binder Tye	Capacity Loss per Cycle/%	C Rate	C Rate in mA g^{-1}	References
dopamine-modified CMC	Anode	0.19 *	0.293 *	1000	[143]
P-HAEAPMA	Anode	0.0826 *	0.2	-	[144]
PGB	Both	0.0925 *	10	-	[146]
PA-PN-PBA-g-CMC	Anode	0.0435 *	0.2	-	[154]
carboxymethyl cellulose and polydopamine	Anode	0.133 *	0.2	-	[148]
Pd(PPh3)(4) catalyst, dibromo benzoic acid, dioctylfluorene-diboronic acid bis(1,3-propanediol) ester.	Anode	0.395 *	-	-	[149]
polyimine binder	Anode	0.0176 *	2.49 *	2000	[150]
	Anode	0.098 *	0.189 *	400	[150]
bPAA-3	Anode	0.24 *	0.5	-	[151]
palladium-catalyzed direct arylation of 3-(2-ethylh exhyl) thiophene or 3,3′-di(2-ethylhexyl)bithiophene and dimethyl-2,5-dibromoterephthalate, followed by saponification.	Anode	0.048 *	1	-	[152]

* Values with [*] are calculated using data from the literature sources but not directly stated in the article.

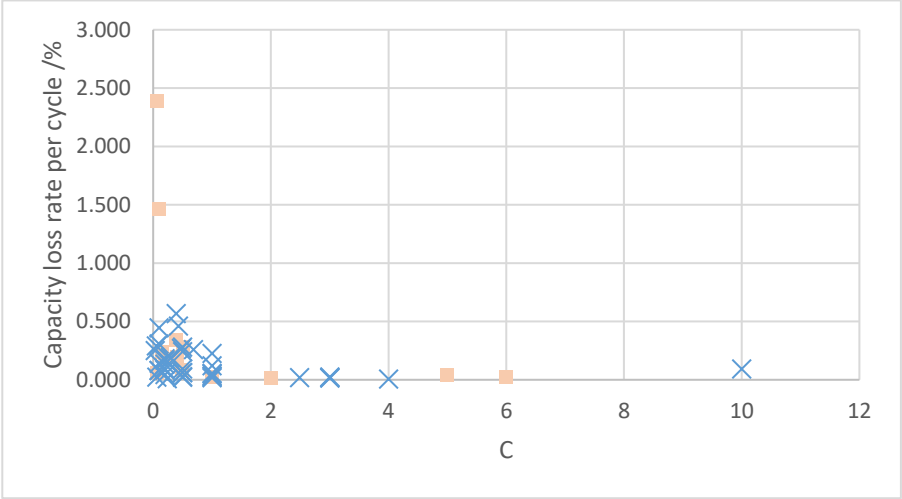

Figure 20. Plot of capacity loss per cycle against C testing conditions for other polymeric binders (blue cross) in comparison with green binders (light orange square), based on data from Table 9 [111–128,130–136,138–146,148–154].

Comparing the initial capacities and rate of capacity loss per cycle, other polymeric binders seem to have a comparable performance to green binders in general, regardless of the anode system, though notably there are a few anomalies for green binders. In terms of the binder types, anodic binders seem to be more investigated compared to cathodic binders, and generally much higher initial capacities are reported, with many reaching capacities of over 1000 mAh g^{-1}. This may be largely due to the electrodes that were used in testing, as many anodic binders have a strong focus on addressing the drawbacks of Si anodes, while cathodic binders were tested under different conditions (e.g., $LiFePO_4$/Li half-cell [112]).

Similar trends for binder functional groups and cross-linked structures are also observed among binders for LIBs, suggesting that similar strategies can be used across various Li-based battery types. The investigation of optimized Si/PAAS6-β-CDp1-PAA3 electrode yielded the highest reported initial discharge capacity of 3869 mAh g^{-1}, with its performance attributed to features that were present in many other novel binders, namely strong adhesion due to numerous functional groups as well as the effective accommodation of volume expansion, likely due to the effect of cross-linking [138].

Following from the observations made for Li-S binders, modifications to PAA and CMC are also utilized frequently in replacement of traditional PVDF binders, with strategies of grafting, copolymerization and cross-linking, giving the resultant binder enhanced properties such as flame retardation [145], improved mechanical toughness [141], and improved stability and adhesion [123].

Notably, the palladium catalysis of binders has also been explored in recent years, with its usage applied to the direct arylation of 3-(2-ethylhexhyl)thiophene and 3,3′-di(2-ethylhexyl)bithiophene and dimethyl-2,5-dibromoterephthalate, followed by saponification, simplifying the preparation procedure of the binder while reducing cost and minimizing environmental impact [152]. The Pd (PPh3)4 catalyst was also utilized to facilitate the Suzuki polycondensation reaction between dibromo benzoic acid and dioctylfluorene-diboronic acid bis(1,3-propanediol) ester, resulting in a gel polymer with multi-functionality [149].

In addition, several binders are also effective in mitigating the effects of the large volume fluctuations in Si electrodes. It has been noted that 1D chain polymers are often not optimal for Si anodes as they are unable to withstand these volume changes due to insufficient mechanical properties [23]. However, the formation of physically cross-linked 3D networks with reversible bonding effects (rather than chemical cross-linking via covalent bonds) was found to better accommodate these volume changes and improve cyclability [23], as well as imparting self-healing properties, as demonstrated by the PFA-TPU binder system [117].

From the overall review of these binder designs, several design strategies are presented in order to improve properties such as the cohesion and mechanical resilience of the binders and electrodes. Polar hydroxyl groups are particularly effective in improving the adhesion of the binders to the electrode surface, as demonstrated by the use of sesbania gum (SG) on silicon nanoparticles, where strong adhesions was deduced to form between the silanol group (Si-OH, where O acts as a proton-acceptor) and the -OH and -COOH groups in the binder that act as proton donors [102].

Cross-linking between polymers is also a common strategy to address mechanical resilience as it prevents the disentanglement of the binder chains during volumetric expansions of the anode [141]. Notably, the existence of both hydroxyl and carboxylic groups in the copolymers is advantageous for the cross-linking process due to their ability to form covalent networks [141].

3.1.4. Other Li Batteries

While most research was conducted on LIBs and Li-S batteries, notable developments were also seen for binders for other lithium battery types, such as Li-O_2 batteries, Li-Se batteries and solid-state batteries (Table 10).

The focus on environmentally friendly binders lead to the development of lithium carboxymethyl cellulose, CMC-Li, as a water-soluble alternative to PVDF in Li-O_2 batteries. Compared to commercial versions that utilize sodium (CMC-Na), the Li-modified version showed improved discharge specific capacities of 11,151 mAh g^{-1} at 100 mA g^{-1} and a cycling stability of 100 cycles at 200 mA g^{-1}, attributed to the enhanced diffusion of Li ions in the cathode. This displays the potential for such binders to replace PVDF in Li-O_2

batteries [156]. Novel alternatives are also proposed to replace PVDF in Li-Se batteries, which face similar issues to Li-S batteries (i.e., volume expansion and the shuttle effects of poly-selenides). Okra gum was explored as a green alternative, and showed promising results, with superior initial discharge capacity (607 mAh g^{-1} at 0.2 C), cycling stability (218 mA h g^{-1} after 100 cycles at 0.2 C), and rate performance (364 mA h g^{-1} at 1 C) compared to Li-Se batteries with traditional PVDF binders. This also demonstrates the potential of using natural plant-based materials in battery designs, similar to the usage of various plant-based gums, as mentioned for Li-S binders [155].

Table 10. Data obtained for initial capacities and capacity loss per cycle at various C rate conditions for the binders of other Li-based batteries. (Note that in addition to C rates, there are also other testing conditions, such as cycling voltage, that may differ across articles; hence, the comparisons are only approximate).

Battery Type	Binder	Initial Capacities/mAh g^{-1}	C Rate (for Capacities)	Capacity Loss per Cycle/%	C Rate (for Capacity Loss)	Reference
Li-Se	okra gum (OG)	607	0.2	0.641 *	0.2	[155]
Li-O_2	Lithium-ion modified cellulose (CMC-Li)	11,151	1 A g^{-1}	-	-	[156]
Solid-state	poly(3,4-ethylenedioxythiophene)/poly(4-styrenesulfonate) (LFP) cell with 10.0 wt. % OMIECs	145	1	0.0193 *	1	[157]
Solid-state	polybutadiene and acrylonitrile-butadiene rubbers (NBR)	149	0.2	0.158 *	0.2	[158]
Solid-State	poly(tetrafluoroethylene-co-perfluoro(3-oxa-4-pentenesulfonic acid)) lithium salt	180.7	0.1	0.0333 *	0.5	[159]

* Values with [*] are calculated using data from the literature sources but not directly stated in the article.

Various polymeric binders for solid-state batteries were also explored in recent years, with the overall goal to improve ionic conductivity and maintain stable interfaces between components [157,158]. Among the binders explored, an ionomeric binder utilizing poly(tetrafluoroethylene-co-perfluoro(3-oxa-4-pentenesulfonic acid)) lithium salt achieved the highest discharge capacity, at 180.7 mAh g^{-1} (3.05 mAh cm^{-2}) at 0.1 C, with the performance attributed to its ability to promote Li+ transportation and its even distribution on the electrode [159].

3.2. Alternative Slurry Processes

3.2.1. Dispersants and Additives

The various articles assessed for slurry synthesis and utilization can be categorized into several types, namely the introduction of dispersants and additives, and alternative preparation reagents and/or methods.

The introduction of dispersants and additives the slurry synthesis seems to have attracted significant interest in recent years, stemming from the goal of improving the quality of electrode coatings for various battery types. For example, the addition of a copolymer P(VP-AA-AM) dispersant to a lithium manganese iron phosphate (LMFP) cathode slurry for Li-ion batteries greatly improves the uniformity and stability of the active materials in the slurry. This can be attributed to the adsorption of the P(VP-AA-AM) copolymer onto LMFP nanoparticles, which in turn results in an improvement in rate performance and cycling performance in the cell [160]. A similar strategy can be used for the slurry process for polyethylene (PE) separators, where the addition of premixed heterogeneous ceramics such as silica (SiO_2) and alumina (Al_2O_3) in an aqueous solution

results in improved dispersion stability due to the electrostatic repulsion between the SiO_2 sheaths that surround the Al_2O_3 particles. This translates to improved wettability, ionic conductivity, and uniform ionic flux, which improves the electrochemical performance of the battery [161].

Introducing additives into the slurry process can also serve other purposes. Notably, the addition of various carboxylic acids to the low-pH slurry preparation of silicon electrodes (in Li-ion batteries) can serve as a buffer solution, and maintaining a small amount (5 wt.%) in the solution can lead to reduction in the amount of inactive material in the solution, hence increasing the energy capabilities of the resultant cell [162]. Furthermore, some additives, such as 4-(ethoxy) trimethylolpropane tri-acrylate (EOTA), can serve as multifunctional components in slurry preparation, designed to protect electrodes such as NCM811 from potential side reactions as well as enhancing lithium–ion transport kinetics at the electrolyte–electrode interface. Hence, the efficient choice of components can both improve the structural integrity of the electrode by slowing corrosion and improving its electrochemical capabilities at the same time [163].

3.2.2. Alternative Methods and Scalability

Improving the electrochemical properties of the battery does not always require changes in the material. Recently, alternative methods have been developed to improve physical properties of electrodes such as flexibility and performance. This is particularly effective in the synthesis of thick electrodes for high-performance Li-S batteries, where controlled cracking was used to provide channels for ionic diffusion and accommodate fluctuations in volume during charging cycles while maintaining a high energy density (560 Wh kg^{-1}). Paired with enhanced mechanical properties, its simple fabrication process and wide application to other active components showcases the potential of exploring alternative processing methods in improving battery capabilities [164]. It was also found that simply changing the mixing order of slurry components can have profound effects on the resultant electrode properties due to the interactions between different components as they are added. For example, the optimized sequence to produce uniform ceramic-coated separators for Li-secondary batteries was inferred to be premixing the ceramics and surfactants before the addition of the binder, as the surfactants provide strong steric repulsions that enhance dispersion stability and ensure even coating. This in turn improves various electrochemical factors of the resultant battery [165].

While improving the electrochemical properties of the battery is desirable, the scalability of the coating synthesis is also an important factor to consider when assessing the applicability of battery designs for commercial use. In recent years, there has been increasing focus on investigating the feasibility of various novel components for commercial-scale production, particularly for solid-state type batteries, where large-scale production is limited by the sensitivity of components to air [166], polar solvents and moisture [167]. For example, sheet-type $LiNi_{0.88}Co_{0.10}Al_{0.02}$ (NCA) cathodes with an island-like amorphous Li_2O–ZrO_2 (LZO) coating layer have been successfully produced at a large scale via the wet slurry process, using PVDF-HFP (acting as a binder) dissolved in butyl butyrate. This was done while still maintaining its remarkable capacity and retention (initial areal capacity of 2.936 mAh cm^{-2} at 0.64C and capacity retention of 69.93% after 1000 cycles at room temperature), demonstrating potential for commercial application [168].

Increasing concern regarding the environmental impacts of battery production has also led to more interest in exploring water-based slurry synthesis for various battery components in recent years. Ideally, the electrochemical properties of the component would be maintained or enhanced while negating the negative impacts of traditional organic solvents. This is especially so for cathodes, where PVDF and NMP are still commonly

used [169]. However, recent advances have seen the preparation of thick LFP cathodes with embroidered current collectors, achieving superior performance (more than 1.5 times greater in energy density) to conventional electrodes, and hence demonstrating the feasibility of utilizing a water-based slurry for production [169]. Furthermore, the use of water-based slurries can also be applicable to other battery components, namely separators. Once again, PAA-based binders seem to be a promising alternative to water-based slurries, with a stronger bonding ability and superior thermal stability relative to traditional PVDF when used in Al_2O_3 composite separators [10]. The replacement of the NMP solvent was also explored using other novel techniques, such as photopolymerization, using ethylene carbonate/dimethyl carbonate as a photoactive electrolyte solvent, yielding electrodes with higher porosity and wettability properties [170].

With regard to the promising binder designs noted in previous sections, processes such as grafting, cross-linking, and copolymerization are common in the synthesis of many binders. Hence, when assessing the ease of integrating these binders into industrial production, the scalability of these chemical reactions is a crucial aspect to consider. Notably, bond-forming processes such as copolymerization could be exothermic and can often result in thermal runaways, especially in the context of upscaled, industrial production [171]. As such, temperature control could present a challenge in the synthesis of these binders in large batches, and precise control would be required for any in situ synthesis of the binders at the battery slurry stage, as increased temperature would reduce the viscosity of the slurry [172], and may hence affect the subsequent stages of coating and calendaring.

3.3. Alternative Manufacturing Processes and Recycling Assessments

3.3.1. Incorporation of Technology and Digitalization

Given the advancements in technology and the introduction of Industry 4.0 [173] in recent years, the incorporation of these technologies into the battery manufacturing framework has much potential for boosting the efficiency of production as well as reducing the cost. There are four main processing steps in LIB production: slurry-mixing, coating, drying, and calendaring [174], as shown in Figure 21.

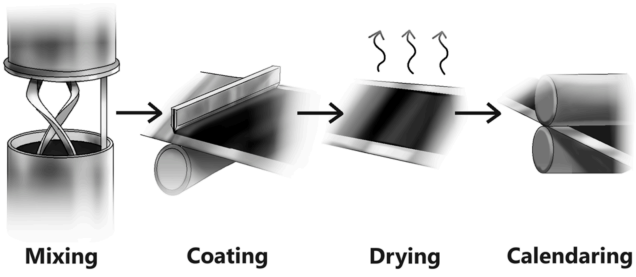

Figure 21. Diagram illustrating the main processing stages of LIB production.

Due to the interdependent kinetics of the chemistry of LIBs, the production system of LIBs is complex [174], with numerous factors that affect the effectiveness of each production stage. For example, mixing (and hence slurry quality) is dependent on duration, mixing and rotational speed, and degassing time, while drying is dependent on temperature profile. Coating and calendaring also require an optimal speed of application to ensure the best quality of the battery component [173]. As a result, traditional manufacturing methods are limited by inefficiencies in its trial-and-error approach, resulting in inconsistencies in processing, material wastage and inflated production cost [175]. The inconsistencies in production can in turn have adverse impacts on the resultant battery performance [176]. Furthermore, the current production of LIBs and electricity still depends heavily on fossil fuels [177], with recent research showing that the largest contributor to environmental

impact, e.g., Global Warming Potential, is active material production, further emphasizing the need to consider environmental factors in the context of battery design choices [178].

Fortunately, with the advancements in technology, the manufacturing process can be streamlined through the digitalization and utilization of Artificial Intelligence (AI). Through this integration, traditional quality-control methods can be replaced by AI machine vision for the detection of defects, which can be achieved with training data to allow the model to effectively predict defects through images or videos at a web speed of 9 ms^{-1}, and is hence especially useful for identifying defects in the coating and calendaring stages [179]. Machine Learning (ML) can also be incorporated to ensure optimal slurry composition and even the coating of electrodes through analyzing relevant parameters in these steps and using the most appropriate processing conditions for homogeneity [180], as opposed to traditional physics-based models, in turn improving the quality, consistency and efficiency of manufacturing, as well as enhancing the scalability and sustainability of the process through automation [175]. With the use of ML based on self-organization mapping (SOM) neural networks, the performance of resultant battery packs has seen notable improvements, with a 1.9% increase in capacity and a reduction of 4–5 °C and 2.6 °C in peak temperature and temperature fluctuations, respectively [176]. Furthermore, digitalization can aid in battery prototype designs, reducing the prototyping costs [174]. Recent developments in the incorporation of deep-learning into the production framework also saw the proposal of a four-step hybrid detection model to monitor real-time production performance and ensure sustainable manufacturing. Implementation showed promising results with very high accuracy, significantly reducing production time (negating manual testing time and saving approximately 3.5 h per battery pack), demonstrating its profound impact on the efficiency of production [181].

To further streamline the process, digitalization can be tailored to have more focus on the steps that are essential to ensure the quality of batteries, considering the ease of digitalization. This strategy ensures the quality of the LIBs produced while reducing the number of parameters that need to be digitalized. More importantly, it priorities parameters based on their effects on the quality of the final product, compiling parameter lists for each of the manufacturing processes, from slurry-mixing to calendaring [173]. Digitalization can be further optimized with the use of force field (FF) parametrization, where the properties of slurries with various compositions can be simulated, allowing for accelerated screening for different fabrication conditions [182].

3.3.2. Alternative Manufacturing Methods

In recent years, many alternative manufacturing methods have been developed to enhance the production of LIBs. Among the various additive manufacturing methods proposed [183], 3D printing technology has been regarded as a promising tool for incorporation, being able to produce complex structures and custom designs, which in turn ensures the electrochemical performance of resultant batteries. Furthermore, the technique is cost-effective and highly efficient, and has been successfully used to produce various Li-based batteries, including LIBs, Li-S and Li solid-state batteries [184]. The versatility of 3D printing can also be applied to novel battery designs. With regard to a proposed 3D-aligned architecture design for batteries, the 3D printing method for composite electrodes and electrolytes was seen to produce precise and controlled structures, displaying potential for such applications [185]. Similar techniques can be combined with nanomaterial orientation to produce thick electrodes with out-of-plane aligned architecture, yielding electrodes with more than twice the capacity of slurry-cast ones [186].

In addition to applications in the batteries themselves, 3D printing technology can also be utilized to produce tools to assist in battery assembly. For example, 3D printing has

been used to address the issue of alignment in coin cells, where precise alignment is crucial to ensuring electrochemical performance. A 3D-printable design for a coin cell alignment device was made to accelerate the lab-scale battery assembly process, significantly reducing the time taken by up to 35% relative to manual alignment. Furthermore, the resultant coin cell displayed superior electrochemical properties, with an increase of 150 mAh g^{-1} in average discharge capacities and up to a 2.0% increase in Coulombic efficiency [187]. The use of bio-derived filaments (PLA) in FDM-sintering processes has also been explored, enabling the fabrication of solid-state electrolytes with an ionic conductivity of 2.529×10^{-5} cm^{-1}, supporting fully recyclable component designs while reducing material waste [188].

However, 3D printing techniques face a major challenge in commercial large-scale production due to their poor scalability as opposed to other methods that have cost and efficiency advantages in this regard [185]. Furthermore, the consistency and performance stability of each individual 3D-printed battery becomes a concern when considering industrial-scale production, coupled with the material waste and insufficient mechanical strength [184]. The current applications of 3D printing are therefore still limited to lab-based settings, with strategies for implementation on an industrial scale remaining to be explored.

Existing steps in the LIBs manufacturing process can also be truncated or combined to improve the efficiency of production. For raw materials' extraction, traditional lithium extraction and purification can be combined using a coupled electrochemical technique. The process is one-step and can extract battery-grade lithium to be directly used in manufacturing, hence bypassing the traditional extraction and purification steps and producing economically superior cathodes [189]. Novel fabrication techniques were also explored for all-solid-state lithium batteries, where electrolytes with low melting points were used to infiltrate solid electrodes to produce low-porosity electrode–electrolyte interfaces, negating the sintering step that is traditionally used. Furthermore, it was proposed that the melt-infiltration technique is applicable to other similar solid-state electrolytes utilizing nearly the same equipment, hence demonstrating its high versatility and ease of industrial adoption [190]. Similarly, the dewatering technique was proposed for the accelerated production of LIBs from the slurry to coating steps by casting the slurry onto a porous mold, separating the solvent using negative pressure or gravity rather than extraction via evaporation solvent, resulting in a substantial reduction in processing time [191].

With the increasing concerns regarding environmental and human impacts, the industry has been moving away from discrete, solvent-based steps toward integrated, additive processes. Such change mainly stems from the need to avoid the toxic organic solvents used in traditional methods. Furthermore, the lack of solvents in these alternatives negates the need for electrode-drying and solvent-recovery steps, reducing production costs while improving electrochemical performance. Solvent-free manufacturing via binder fibrillation, among other methods, represents a paradigm shift, with the LFP-based batteries produced having achieved areal discharge capacities of 2.1 to 6.4 mAh cm^{-2} and a maximum specific discharge capability of approximately 150 mAh g^{-1} [192]. Other solvent-free methods such as dry-printing were developed for coating the active material on the current collected, yielding a unique resultant microstructure that leads to improved charging capabilities (70% at 4C, compared to 52% for the reference) and lengthened cycle life [193]. Hence, solvent-free manufacturing methods can be a promising alternative for future production, given their scalability and environmental considerations, as well as their versatility, since many methods allow for one piece of equipment to be used to produce various components [194].

Similar considerations lead to investigations into implementation of "Li-free" manufacturing through in situ plating of Li anode, which also addresses issues of scalability when working with bulk Li or ones by vapor deposition [195].

3.3.3. Recycling and Environmental Impact Assessments

In the pursuit of performance, laboratory-scale research often overlooks the environmental cost of material synthesis. In the case of lithium–oxygen cathodes, recent studies on reduced-graphene oxide/alpha-manganese oxide/palladium (rGO/-MnO_2/Pd) cathodes report an exceptional specific capacity of 7500 mAh g^{-1}. However, the synthesis of these materials is a chemically intensive process involving sulfuric acid, sodium borohydride, and hydrogen peroxide. The resulting GWP of 1130.71 kg CO_2 per kg of active material presents a staggering environmental debt compared to conventional LFP and NMC chemistries [178]. Hence, an optimal balance needs to be reached between the electrochemical performance and environmental impact of battery designs, focusing on lower-impact synthesis pathways without sacrificing the electrochemical gains of graphene-based architectures, leading to a performance–sustainability paradox.

With the increasingly prevalent usage of lithium-based batteries, end-of-life processes for these batteries, their recycling strategies, and the environmental impact of their disposal become important for assessment. Hence, detailed Life Cycle Assessments (LCA) are crucial to understand the emissions of LIBs during production, usage and disposal, with the goal of achieving sustainability. It was found via a cradle-to-gate approach that the recycling of metal components is crucial in pursuing a circular economy, with a reduction in raw metallic materials having a significant lowering effect on the overall environmental assessments [196]. While the environmental impacts of other components such as graphite anodes are less known due to the lack of industrial data, new Life Cycle Inventory (LCI) for the carbon footprint was suggested based on a review of the data on synthetic graphite; however, notably, reported values tend to be an underestimate [197].

On the topic of recycling and recovery, direct recycling can retain the structure of active materials in the electrodes, hence reducing energy consumption and environmental impact as this minimizes the need for reprocessing. It is effective in the recovery of important components such as lithium iron phosphate (LFP) and lithium nickel manganese cobalt oxide (NMC) from cathodes without degradation, while maintaining a low recovery cost that can compete with the prices of virgin materials. Furthermore, it has been shown that slurry electrolysis can be used to further separate metal components such as Li, Mn and Fe from spent cathodes, with high rates of recovery (89.83%, 88.69% and 94.42%, respectively) [198]. Being efficient and environmentally friendly, this technique also has notable potential on an industrial scale, allowing these metal components to be repurposed for other applications, such as photocatalysts [199]. The components of batteries have also been shown to be recoverable from other sources, such as biogas slurry, which yields battery-grade $FePO_4$ via a low-carbon-emitting Fe-cycle strategy, while maintaining lower cost and carbon emissions compared to industrially produced components (5.42 $/kg P, CO_2 emissions of 80.83 kg/kg P, compared to 14.60 $/kg P and 110.60 kg/kg P) [200].

Moreover, direct recycling produces the lowest greenhouse gas emissions compared to thermal recycling (1.18 kg CO_2 at 200 °C to 2.02 kg CO_2 at 400 °C for LFP, 6.98 kg CO_2 at 200 °C to 1.94 kg CO_2 at 400 °C for NMC), showing great potential for scalability and applications such as on-site recycling [201].

Considering the major candidates for binder functionalities that were mentioned in previous sections, their ease of recycling and their respective end-of-life processes are also an important aspect in the design of environmentally friendly batteries. Amide functional groups, which were previously shown to improve redox kinetics in Li-S batteries, were found to be easily broken down into monomers via the process of hydrolysis despite their high bond strength, which in turn makes it easy for them to be separated from the electrodes and potentially be extracted for re-synthesis. Furthermore, it was noted that while strong bond formations are desirable for the enhancement of several binder properties

(i.e., mechanical resilience, adhesion strength and retention of active species), they could also become an issue in the recycling stage due to the lack of solubility and difficulties extracting them using a solvent [202]. Fortunately, as many binders rely on hydrogen bonding interactions between hydroxyl or carboxyl groups, with electrode and active materials being used to facilitate ion transport and adhesion, while others like zwitterionic binders rely on ionic interactions for self-healing properties, the main intermolecular interactions that give rise to the desired binder improvements can be categorized in terms of hydrogen and ionic bonding. These bonds can be dissociated at high temperatures, allowing them to dissolve quickly in water, and hence making the direct recycling of these binder choices economically and chemically feasible [203].

4. Recent Developments

While much research has already been conducted with regard to battery binders and processes in the selected time scope of 2020 to 2025, there are still numerous ongoing developments in this field. Notably, there is more diversification of battery designs, moving away from binders and electrodes and revisiting the use of lithium metal anodes. The incorporation of composite solid electrolytes with the use of Co-, Cu- and Sn-doped $Li_{1.5}Al_{0.5}Ti_{1.5}(PO_4)_3$ (LATP) powders in the polymer mixture was found to enhance the electrochemical stability of the battery over a large voltage range in comparison to conventional Li/Li+ batteries. Sn was found to be the most effective as a doping metal, achieving a superior cycling stability and high energy density, which was attributed to its electronegativity [204].

There are also more developments on binders, with the focus on the recyclability of the binder choice, addressing electrochemical performance as well as proposing potential recycling strategies that were shown to be viable and applicable at large scales. A natural sericin protein with sulfuric acid was investigated as a cross-linked, water-soluble binder with the aim of replacing conventional PVDF binders with a comparable but easily recyclable binder. It was found that soaking it in water at 50 °C for less than 1 min was sufficient for the binder to dissolve, separating the electrode and active materials such that each component can be recycled [203].

Furthermore, alternative manufacturing methods have also been further explored to further reduce the material and environmental costs in manufacturing, with investigations into additive manufacturing strategies such as binder jetting, which has the advantage of reducing the amount of solvent required for electrodes in comparison to traditional tape-casting techniques while maintaining a promising specific capacity of 161.8 mAh g^{-1} [205].

5. Limitations

While the research on lithium-based batteries in recent years has been extensive, and every effort has been made to distill the information from the literature, there are also several limitations to this study.

Considering the assessment of the performance of binders, it was quite difficult to definitively compare their relative performance due to the varying testing conditions for C as well as the large variety of positive and negative electrode combinations that were used in the articles. Many of the binders with a notable performance were tested under relatively low C rates (usually less than 2 C), and since there is limited accuracy when comparing binders across different C rate ranges, their relative ranking among other binders can only be made for others with similar C rates. Hence, the performance comparisons are only a rough approximation. It would be useful to have a future standardization of testing conditions for the easier comparison of data from different laboratories/testing facilities. This would also be useful to standardize the various parameters (e.g., units) that could

be used to determine the relative performance of the binders, such as capacity loss per cycle and initial discharge capacity, as not all the articles assessed contain this specific information. (In this case, specific capacity was not always known, and initial discharge capacity was taken to calculate the C-rate from units in mA g^{-1}, leading to limited accuracy.) In addition, the calculations of capacity loss per cycle used only the average value of the number of cycles and was limited to the range reported in the literature, which could lead to significant error margins for testing conditions with only a small number of cycles. The articles assessed in this review have cycle numbers ranging from 50 to 2000 cycles; hence, there could be considerable uncertainty in the calculated values.

It is also important to note that many of the binders that were assessed in this review were tested at laboratory scale, and under varying testing conditions. Hence, their effectiveness may differ if the battery components were upscaled to larger sizes for industrial or commercial integration, where parameters such as dimension and composition may need to be recalibrated. Additionally, many of the binders with notable performances were tested under relatively low C rates (usually less than 2 C), and since there is limited accuracy in the comparison of binders across different C rate ranges, their relative ranking among compared to other binders is only relevant for others with similar C rates.

Furthermore, due to the wide application of lithium-based batteries (and their binders), the usage of the battery could also affect the parameters that are important when assessing the electrochemical performance of the binder. For example, for stationary LIBs battery weight would be less of a concern compared to LIBs that are installed on moving vehicles. As a result, further consideration regarding the purpose of the battery would be useful in determining the suitability of each binder choice.

6. Conclusions

The research on lithium batteries has been extensive in recent years, covering a large range of battery types and various binder strategies. Notably, the interactions of polar functional groups with the active species in Li-S batteries is an effective strategy that is widely employed for binders to minimize the shuttle effect of soluble polysulfides, extending the cycling stability of Li-S batteries and increasing their electrochemical performance. The shuttle effect can be further reduced for binders that are able to improve the reduction kinetics of the polysulfide species. Further research could benefit from consideration of functional group interactions as well as the ability to facilitate redox kinetics, specifically the incorporation of amide, hydroxyl and carboxyl groups. Alternatively, other polar groups and charged species could also be explored, with a focus on their ability to form hydrogen bonds or ionic interactions.

Properties such as a high modulus and self-healing properties mitigate the effects of volume changes and enhance cycling stability, which are applicable across various battery types, with binders that are zwitterionic being a promising option for further research. Further exploration of other binders that interact via ionic bonding can be considered, and their modulus and self-healing properties could potentially be compared.

Furthermore, with regard to research on novel binder alternatives, the feasibility of these novel binders being incorporated into current LIB production, the ease of their synthesis at an industrial scale, and their possible end-of-life processes and environmental impacts are also useful considerations when assessing suitability.

With regard to manufacturing and recycling, it is apparent that the production of batteries has a profound impact on climate change, both through the components used and the processing required for the synthesis or extraction of raw materials. While much has been explored with regard to automation and the incorporation of technology such as 3D printing and additive manufacturing to minimize the impact of production, the environmental

impacts of recycling various components of Li-based batteries could be further investigated, especially recycling strategies for smaller components, such as binders, active materials and separators. Furthermore, alternative battery designs (such as a recyclable or sustainable design) to achieve an optimal balance between performance and eco-friendliness could also be further explored to address the performance–sustainability paradox.

Author Contributions: Conceptualization, J.L. and S.P.; methodology, J.L.; software, J.L.; validation, J.L. and S.P.; formal analysis, J.L.; investigation, J.L.; resources, S.P.; data curation, J.L.; writing—original draft preparation, J.L.; writing—review and editing, J.L. and S.P.; visualization, J.L.; supervision, S.P.; project administration, S.P.; funding acquisition, S.P. All authors have read and agreed to the published version of the manuscript.

Funding: This research received no external funding.

Data Availability Statement: No new data were created or analyzed in this study. Data sharing is not applicable to this article. All data supporting the findings of this review are derived from the literature cited in the reference section. Further information can be found by contacting the corresponding author.

Acknowledgments: During the preparation of this manuscript/study, the authors used Krita ver. 5.3 for the purpose of diagram illustrations and Microsoft Excel for the purpose of creating the graph plots. The authors have reviewed and edited the output and take full responsibility for the content of this publication.

Conflicts of Interest: Author Shiladitya Paul was employed by the company TWI. The remaining author declares that the research was conducted in the absence of any commercial or financial relationships that could be construed as a potential conflict of interest.

Abbreviations

The following abbreviations are used in this manuscript:

GHG	greenhouse gas
IC	internal combustion
EV	electric vehicles
LIB	lithium-ion battery
VOC	volatile organic content
PVDF	polyvinylidene fluoride
NMP	n-methyl pyrrolidone
AG	aloe vera gel
PA	phytic acid
BA	boric acid
RG	ramie gum
LSO	lithium polysilicate
TPG	tamarind polysaccharide gum
CMC	carboxymethylcellulose
PAA	polyacrylic acid
XG	xanthan gum
WPUP	waterborne polyurethane polymer with phytic acid
HPRN	hydroxypropyl poly-rotaxane
SPI	soybean protein isolate
PEO	poly(ethylene oxide)
MAR	Methylated amino resin
NACCTS	N-acetyl-L-cysteine-chitosan
CRP	Curdiea racovitzae-derived polysaccharide
RB	Ramie gum with boric acid
TFSI	bis(trifluoromethanesulfonyl)imide

PAM	polyacrylamide
PTPO	3D cross-linked polyether binder
ICEP	ionically conductive elastic polymer
PVA	poly(vinyl alcohol)
PAAMPS	poly 2-acrylamido 2-methyl 1-propane sulfonic acid
PLM	lipoic acid and zwitterionic monomer 2-methacryloyloxyethyl phosphorylcholine
LPM	lipoic acid, polyethylene glycol diacrylate, 2-methacryloyloxyethyl phosphorylcholine
PIL	cationic imidazole group on polymethyl methacrylate backbone
AP	polymeric aluminophosphate
HMM	hexamethylolmelamine
LA	lipoic acid
GA	gallic acid
β-CDp	β-cyclodextrin polymer
Cg	choline glycerophosphate
2AD	two adamantane units
TA	tartaric acid
PEI	polyethyleneimine
PLG	polyacrylamide, locust bean gum and gellan gum
PGA	polyglutamic acid
SBMA	sulfobetaine methacrylate
PEGA	poly(ethylene glycol) methyl ether acrylate
HEA	2-hydroxyethyl acrylate
PVP	polyvinylpyrrolidone
CA	citric acid
CPAM	cationic polyacrylamide
HBPE	hyperbranched polyester
c-QACS	cross-linked quaternary ammonium cationic starch
CCSN	Cross-linked chitosan sulfate network
P4VC	poly(4-vinyl catechol)
XNBR	carboxylated acrylonitrile-butadiene rubber
rGO	reduced graphene oxide
DICP	ionic cross-linked polymer (PAA and PEI)
BPI	benzo(ghi)perylene imide
HMT-PMBI(I-)	poly[2,2′-(2,2″,4,4″,6,6″-hexamethyl-p-terphenyl-3,3″-diyl)-5,5′-bibenzimidazolium iodide]
PETU	Poly(ether-thioureas)
PEDOT	poly(3,4-ethylenedioxythiophene)
PSS	poly(styrenesulfonate)
HPAA	hyperbranched poly(amidoamine)
CLE	cellulose levulinate ester
GG	guar gum
TOCNF	cellulose nanofiber
SA	sodium alginate
PEG	polyethylene glycol
TKP	tamarind kernel powder
SG	sesbania gum
PSSTFSI	poly[(4-styrenesulfonyl) (trifluoromethylsulfonyl) imide]
PPC	polypropylene carbonate
PTMC	poly(trimethylene carbonate)
PE	polyethene
AA	acrylic acid
SBR	styrene–butadiene rubber

ZIPs	Sulfobetaine methac-rylate and poly(ethylene glycol) methyl ether methac-rylate zwitterionic polymers
PSFB	polyspirobifluorene-based binder
MA	malonic acid
PTA	polylipoic acid
PMAI	poly(oxycarbonylmethylene 1-allyl-3-methyimidazolium)
WPU	waterborne polyurethane
PU	polyurethane
TMPU	cross-linked MDI-based waterborne polyurethane
PPC-P	poly (propylene carbonate)-plus
BDSA	(1,1′-biphenyl)-4,4′-diamino-2,2′-disulfonic acid
DPA	3,3′-dithiodipropionic acid
PEGCE	poly(ethylene glycol) bis(carboxymethyl) ether
TA-PEDOT:PSS	tannic acid with PEDOT:PSS
MG49	poly(methyl methac-rylate)grafted natural rubber
PBDT	poly(2,2′-disulfonyl-4,4′-benzidine tereph-thalamide)
PGB	biopolymer chitosan, 1-butyl-1-methylpyrrolidinium dicyanamide (PYR(14)DCA) ionic liquid and the lithium bis(trifluoromethanesulfonyl)imide salt
C-PAVIm	cross-linked poly(N-allyl-vinyl im-idazolium)
PDADMA	poly(diallyldimethylammonium)
CFSO	nonafluoro-1-butanesulfonate
FSI	bis(fluorolsulfonyl)imide
BETI	bis(perfluoroethylsulfonyl)imide
P-BIAN	poly(bisiminoacenaphthenequinone)
TUEG	poly(ether-thioureas)
P-HAEAPMA	poly(2-propenoic acid, 2-methyl-, 3-[(2-aminoethyl) amino]-2-hydroxypropyl ester)
FREP	flame-retardant epoxy resin
PProDOT-Hx(2)	dihexyl-substituted poly(3,4-propylenedioxythiophene)
bPAA-3	poly(acrylic acid-co-tetra(ethylene glycol) diacrylate)
PA-PN-PBA	poly (acrylic acid-co-N-methylol acrylamide-co-butyl acrylate)
OG	okra gum
LFP	lithium iron phosphate
NBR	polybutadiene and acryloni-trile-butadiene rubbers
OMIEC	organic mixed ionic-electronic conductors
LMFP	lithium manganese iron phosphate
VP	vinylpyrrolidone
AM	acrylamide
EOTA	4-(ethoxy) trimethylolpropane tri-acrylate
NCM	nickel cobalt manganese
HFP	hexafluoropropylene
AI	artificial intelligence
ML	machine learning
FF	force field
PLA	polylactic acid
GWP	Global Warming Potential
NMC	nickel manganese cobalt
LCA	Life Cycle Assessments
LCI	Life Cycle Inventory

References

1. Chang, X. Solid-state lithium-ion batteries for grid energy storage: Opportunities and challenges. *Sci. China-Chem.* **2024**, *67*, 43–66. [CrossRef]
2. Goodenough, J.B.; Kim, Y. Challenges for Rechargeable Li Batteries. *Chem. Mater.* **2010**, *22*, 587–603. [CrossRef]

3. Etacheri, V. Challenges in the development of advanced Li-ion batteries: A review. *Energy Environ. Sci.* **2021**, *4*, 3243–3262. [CrossRef]
4. Armand, M. Lithium-ion batteries—Current state of the art and anticipated developments. *J. Power Sources* **2020**, *2479*, 228708. [CrossRef]
5. Liu, Y.; Yu, J.; Guo, D.; Li, Z.; Su, Y. $Ti_3C_2T_x$ MXene/graphene nanocomposites: Synthesis and application in electrochemical energy storage. *J. Alloys Compd.* **2020**, *815*, 152403. [CrossRef]
6. Huang, S.; Huang, X.; Huang, Y.; He, X.; Zhuo, H.; Chen, S. Rational Design of Effective Binders for $LiFePO_4$ Cathodes. *Polymers* **2021**, *13*, 3146. [CrossRef]
7. Wu, F.X. Guidelines and trends for next-generation rechargeable lithium and lithium-ion batteries. *Chem. Soc. Rev.* **2020**, *49*, 1569–1614. [CrossRef] [PubMed]
8. Lithium-Ion Battery Market (2026–2033): Size, Share & Trends Analysis Report by Product (Lithium Cobalt Oxide, Lithium Iron Phosphate), by Application (Consumer Electronics), by Region, and Segment Forecasts. Available online: https://www.grandviewresearch.com/industry-analysis/lithium-ion-battery-market (accessed on 9 May 2026).
9. Wang, Z.; Zhang, H.; Zhang, X.; Wang, X.; Zhang, X. Solvent-free and large-scale synthesis of SiOx/C nanocomposite with carbon encapsulation for high-performance lithium-ion battery anodes. *Compos. Part B Eng.* **2022**, *247*, 110308. [CrossRef]
10. Xu, R.; Sheng, L.; Gong, H.; Kong, Y.; Yang, Y.; Li, M.; Bai, Y.; Song, S.; Liu, G.; Wang, T.; et al. High-Performance Al_2O_3/PAALi Composite Separator Prepared by Water-Based Slurry for High-Power Density Lithium-Based Battery. *Adv. Eng. Mater.* **2021**, *23*, 2001009. [CrossRef]
11. Tian, Y.; Xie, J.; Tian, M.; Luo, X.; Wang, L.; Zhou, S.; Feng, Y.; Hu, L. Advanced cathode binders for lithium-ion batteries: Molecular design and performance enhancement. *Chem. Eng. J. Adv.* **2025**, *24*, 100838. [CrossRef]
12. Nzereogu, P.U. Anode materials for lithium-ion batteries: A review. *Appl. Surf. Sci. Adv.* **2022**, *9*, 100233. [CrossRef]
13. Thackeray, M.M. Exploiting the Spinel Structure for Li-ion Battery Applications: A Tribute to John B. Goodenough. *Adv. Energy Mater.* **2021**, *11*, 2001117. [CrossRef]
14. Shi, Z. The effect of surface modification on the performance of graphene based honeycomb porous structure as Li-ion battery anode materials. *Comput. Mater. Sci.* **2025**, *246*, 113395. [CrossRef]
15. Sheng, Y.; Wang, Y.; Yin, S.; Zhao, L.; Zhang, X.; Liu, D.; Wen, G. Niobium-Based Oxide for Anode Materials for Lithium-Ion Batteries. *Chem. Eur. J.* **2024**, *30*, e202302865. [CrossRef]
16. Babu, B. Carbon–based Materials for Li-ion Battery. *Batter. Supercaps* **2024**, *7*, e202300537. [CrossRef]
17. Boparai, K.S. Electrochemical Energy Storage Using Batteries, Superconductors and Hybrid Technologies. In *Encyclopedia of Renewable and Sustainable Materials*; Elsevier: Amsterdam, The Netherlands, 2020; pp. 248–254. [CrossRef]
18. Yuan, H.; Huang, J.-Q.; Peng, H.-J.; Titirici, M.-M.; Xiang, R.; Chen, R.; Liu, Q.; Zhang, Q. A Review of Functional Binders in Lithium–Sulfur Batteries. *Adv. Energy Mater.* **2018**, *8*, 1802107. [CrossRef]
19. Guo, R.; Yang, Y.; Huang, X.L.; Zhao, C.; Hu, B.; Huo, F.; Liu, H.K.; Sun, B.; Sun, Z.; Dou, S.X. Recent Advances in Multifunctional Binders for High Sulfur Loading Lithium-Sulfur Batteries. *Adv. Funct. Mater.* **2024**, *34*, 2307108. [CrossRef]
20. Chou, S.L.; Pan, Y.; Wang, J.Z.; Liu, H.K.; Dou, S.X. Small things make a big difference: Binder effects on the performance of Li and Na batteries. *Phys. Chem. Chem. Phys.* **2014**, *16*, 20347–20359. [CrossRef] [PubMed]
21. Wang, Y.-B.; Yang, Q.; Guo, X.; Yang, S.; Chen, A.; Liang, G.-J.; Zhi, C.-Y. Strategies of binder design for high-performance lithium-ion batteries: A mini review. *Rare Met.* **2022**, *41*, 745–761. [CrossRef]
22. Jiang, S.; Zhou, J.; Yang, H.; Tan, S.; Wu, Y.; Wang, C. Ionic liquid fabricated PVDF binder for cathode toward stable and high-rate lithium-ion batteries. *J. Power Sources* **2025**, *633*, 236439. [CrossRef]
23. Kim, S.; Kang, Y.; Han, J.H.; Yeon, S.J.; Min, K.; Kim, T.H. A Polysaccharide Binder with Carbon Quantum Dots for Improved Flexibility of Si Anodes in Lithium–Ion Batteries. *ACS Appl. Energy Mater.* **2024**, *7*, 9806–9815. [CrossRef]
24. Page, M.J.; McKenzie, J.E.; Bossuyt, P.M.; Boutron, I.; Hoffmann, T.C.; Mulrow, C.D.; Shamseer, L.; Tetzlaff, J.M.; Akl, E.A.; Brennan, S.E.; et al. The PRISMA 2020 statement: An updated guideline for reporting systematic reviews. *BMJ* **2021**, *372*, n71. [CrossRef]
25. What is a Battery C-Rate? Definition and Calculations. Available online: https://www.ossila.com/pages/what-is-battery-c-rate (accessed on 29 March 2026).
26. Nitta, N.; Wu, F.; Lee, J.T.; Yushin, G. Li-ion battery materials: Present and future. *Mater. Today* **2015**, *18*, 252–264. [CrossRef]
27. Zhou, G.; Chen, H.; Cui, Y. Formulating energy density for designing practical lithium–sulfur batteries. *Nat. Energy* **2022**, *7*, 312–319. [CrossRef]
28. Li, C. Recent advances in cathode materials for Li–S battery: Structure and performance. *Rare Met.* **2017**, *36*, 365–380. [CrossRef]
29. Kumaresan, K.; Mikhaylik, Y.; White, R.E. A Mathematical Model for a Lithium–Sulfur Cell. *J. Electrochem. Soc.* **2008**, *155*, A576–A582. [CrossRef]
30. Manthiram, A.; Fu, Y.; Chung, S.-H.; Zu, C.; Su, Y.-S. Rechargeable Lithium–Sulfur Batteries. *Chem. Rev.* **2014**, *114*, 11751–11787. [CrossRef]

31. Jung, H.Y.; Jung, H.W.; Koo, M.H.; Hong, T.H.; Kim, D.J.; Lee, J.S.; Lee, Y.H.; Jang, H.; Kim, J.-H.; Kim, S.; et al. An architecting binder derived from Antarctic red algae to accelerate sulfur redox kinetics in Li–S batteries. *Mater. Today* **2025**, *83*, 231–241. [CrossRef]
32. Li, M.; Zhang, J.; Gao, Y.; Wang, X.; Zhang, Y.; Zhang, S. A water-soluble, adhesive and 3D cross-linked polyelectrolyte binder for high-performance lithium–sulfur batteries. *J. Mater. Chem. A* **2021**, *9*, 2375–2384. [CrossRef]
33. Li, G.R.; Wang, S.; Zhang, Y.N.; Li, M.; Chen, Z.W.; Lu, J. Revisiting the Role of Polysulfides in Lithium–Sulfur Batteries. *Adv. Mater.* **2018**, *30*, 1705590. [CrossRef] [PubMed]
34. Liu, S.; Ma, S.; Feng, P.; Liang, F.; Cai, X.; Wang, Y.; Gu, X.; Wang, H. Aloe-Derived Sustainable, Aqueous and Flame Retardant Binder Toward High-Performance Li-S Batteries. *Adv. Energy Mater.* **2025**, *15*, 32. [CrossRef]
35. Ma, S.; Qiu, D.; Zhang, L.; Liu, X.; Ren, X.; Dai, J.; Gu, X.; Hou, Y. An Aqueous, Environmental-Friendly, and Flame-Retardant Biomass-Derived Binder for High-Safe, High-Rate, and Long-Life Lithium–Sulfur Batteries. *Adv. Funct. Mater.* **2025**, *35*, 44. [CrossRef]
36. Ma, S.; Wan, G.; Yan, Z.; Liu, X.; Chen, T.; Wang, X.; Dai, J.; Lin, J.; Liu, T.; Gu, X. Eco-friendly aqueous binder derived from waste ramie for high-performance Li-S battery. *Chin. Chem. Lett.* **2025**, *36*, 5. [CrossRef]
37. Zalka, D.; Vizintin, A.; Maximenko, A.; Pászti, Z.; Dankházi, Z.; Hegedüs, K.; Shankar, L.S.; Kun, R.; Saksl, K.; Fedorková, A.S.; et al. Improving lithium-sulfur battery performance using a polysaccharide binder derived from red algae. *Commun. Mater.* **2025**, *6*, 17. [CrossRef]
38. Kazda, T.; Capková, D.; Jaššo, K.; Straková, A.F.; Shembel, E.; Markevich, A.; Sedlaříková, M. Carrageenan as an Ecological Alternative of Polyvinylidene Difluoride Binder for Li-S Batteries. *Materials* **2021**, *14*, 5578. [CrossRef]
39. Wang, F.; Wan, J.; Liu, J.; Wang, R.; Wang, L. An eco-friendly composite binder with robust network and strong affinity for long-lifespan high-loading Li-S batteries. *Chem. Eng. Sci.* **2023**, *282*, 119294. [CrossRef]
40. Wan, Z.; Huang, Y.; Zeng, X.; Guo, X.; Wu, Z.; Tian, M.; Wu, G.; Ling, M.; Li, Z.; Gao, X.; et al. Peach gum as an efficient binder for high-areal-capacity lithium-sulfur batteries. *Sustain. Mater. Technol.* **2021**, *30*, e00334. [CrossRef]
41. Huang, Y.; Shaibani, M.; Gamot, T.D.; Wang, M.; Jovanović, P.; Cooray, M.C.D.; Mirshekarloo, M.S.; Mulder, R.J.; Medhekar, N.V.; Hill, M.R.; et al. A saccharide-based binder for efficient polysulfide regulations in Li-S batteries. *Nat. Commun.* **2021**, *12*, 5375. [CrossRef] [PubMed]
42. Chuang, Y.-P.; Hong, J.-L. Triple Cross-Linked Network Derived from Xanthan Gum/Sodium Poly(acrylic acid)/Metal Ion as a Functional Binder of the Sulfur Cathode in Lithium-Sulfur Batteries. *ACS Appl. Energy Mater.* **2021**, *4*, 10213–10221. [CrossRef]
43. Man, L.; Yang, Y.; Wang, H.; Wang, Y.; An, Y.; Bao, J.; Wang, C.; Yang, Z. In Situ-Cross-linked Supramolecular Eco-Binders for Improved Capacity and Stability of Lithium-Sulfur Batteries. *ACS Appl. Energy Mater.* **2021**, *4*, 3803–3811. [CrossRef]
44. Wang, H.; Yang, Y.; Zheng, P.; Wang, Y.; Ng, S.-W.; Chen, Y.; Deng, Y.; Zheng, Z.; Wang, C. Water-based phytic acid-crosslinked supramolecular binders for lithium-sulfur batteries. *Chem. Eng. J.* **2020**, *395*, 124981. [CrossRef]
45. Wang, H.; Wang, Y.; Zheng, P.; Yang, Y.; Chen, Y.; Cao, Y.; Deng, Y.; Wang, C. Self-Healing Double-Cross-Linked Supramolecular Binders of a Polyacrylamide-Grafted Soy Protein Isolate for Li-S Batteries. *ACS Sustain. Chem. Eng.* **2020**, *8*, 12799–12808. [CrossRef]
46. Mo, Y.; Wu, Y.; Yin, Z.; Ren, W.; Gao, Z.; Zhang, P.; Lin, J.; Zhou, Y.; Li, J.; Huang, L.; et al. High Cycling Performance Li-S Battery via Fenugreek Gum Binder Through Chemical Bonding of the Binder with Polysulfides in Nanosulfur@CNFs Cathode. *ChemistrySelect* **2020**, *5*, 8969–8979. [CrossRef]
47. Gu, X.; Yang, Z.; Qiao, S.; Shao, C.; Ren, X.; Yang, J. Exploiting methylated amino resin as a multifunctional binder for high-performance lithium-sulfur batteries. *Rare Met.* **2021**, *40*, 529–536. [CrossRef]
48. Jiang, W.; Zhang, T.; Mao, R.; Song, Z.; Liu, S.; Song, C.; Jian, X.; Hu, F. An all-biomaterials-based aqueous binder based on adsorption redox-mediated synergism for advanced lithium-sulfur batteries. *eScience* **2024**, *4*, 100203. [CrossRef]
49. Zou, Y.; Tao, Y.; Wu, Y.; Hu, B.; Yang, C.; Huang, G.; Luo, L.; Yang, M.; Yang, C. Vulcanizable elastomer binders for high areal capacity rechargeable lithium-sulfur battery. *J. Mater. Sci.-Mater. Electron.* **2021**, *32*, 26975–26983. [CrossRef]
50. Shi, Y.; Li, D.; Sun, X.; Xue, Y.; Li, Z.; Fu, Y.; Luo, C.; Lin, Q.; Gui, X.; Xu, K. Cationic Polymer Binder for Simultaneously Propelling Ion Transfer and Promoting Polysulfide Conversion in Lithium-Sulfur Batteries. *ACS Appl. Polym. Mater.* **2024**, *6*, 7430–7440. [CrossRef]
51. Kim, S.; Cho, M.; Lee, Y. Saponin-containing multifunctional binder toward superior long-term cycling stability in Li-S batteries. *J. Mater. Chem. A* **2020**, *8*, 10419–10425. [CrossRef]
52. Zhang, J.; Liang, D.; Huang, G.; Iqbal, S.; Wang, X.; Zhu, X.; Zhao, Y. Epoxy-Ether Network Binder Empowers Ultra-High Sulfur Loading in Practical Lithium-Sulfur Batteries. *Small* **2025**, *21*, e07862. [CrossRef]
53. Han, D.-Y.; Masud; Kim, Y.; Kim, S.; Lee, D.G.; No, J.; Choi, H.C.; Lee, T.K.; Kim, Y.S.; Park, S. Ionically Conductive Elastic Polymer Binder for Ultrahigh Loading Electrode in High-Energy-Density Lithium Batteries. *Adv. Mater.* **2025**, *37*, e2506266. [CrossRef]

54. Kannan, S.K.; Joseph, J.; Hareendrakrishnakumar, H.; Joseph, M.G. Aqueous processable polymer blend as a multifunctional binder for advanced Li-S batteries. *Ionics* **2025**, *31*, 5425–5434. [CrossRef]
55. Lin, X.; Wen, Y.; Ma, D.; Li, J.; Zhu, Z.; Wang, S.; Liu, H.; Xu, X.; Huang, X. A zwitterionic polymer binder Integrating multiple dynamic interactions enables High-Performance Lithium-Sulfur batteries. *Chem. Eng. J.* **2025**, *512*, 162808. [CrossRef]
56. Ma, D.; Wen, Y.; Lin, X.; Li, J.; Zhu, Z.; Wang, S.; Liu, H.; Xu, X. Covalent and non-covalent cross-linked based polymer binders for high-sulfur-loading lithium-sulfur batteries. *Chem. Eng. J.* **2025**, *511*, 162095. [CrossRef]
57. Zheng, H.; Ma, L.; Yi, P.; Fang, Z.; Yuan, Y.; Shen, J.; Ye, M. Multifunctional water-soluble binders for Li-S batteries. *Nanoscale* **2024**, *16*, 20765–20773. [CrossRef]
58. Jian, J.; Chen, Q.; Sun, H.; Li, R.; Hou, Y.; Liu, Y.; Liu, J.; Xie, H.; Zhu, J. Enhancing Li-S battery performance via functional polymer binders for polysulfide inhibition. *J. Energy Chem.* **2024**, *97*, 228–236. [CrossRef]
59. Lin, X.; Liu, X.; Tong, Y.; Zhou, X.; Li, J.; Song, J.; Feng, X.; Liu, R.; Shi, L.; Yu, A.; et al. A Poly(Ionic Liquid)-Based Polymer Binder for Endurable Lithium-Sulfur Batteries. *Adv. Funct. Mater.* **2024**, *34*, 2406985. [CrossRef]
60. Chen, Z.; Chen, T.; Wang, J.; Li, P.; Liu, J.; Chen, W.; Yang, Z.; Deng, Y.; Chang, J.; Yang, Y. A Low-Dosage Flame-Retardant Inorganic Polymer Binder for High-Energy-Density and High-Safety Lithium-Sulfur Batteries. *Adv. Energy Mater.* **2024**, *14*, 2401568. [CrossRef]
61. Liang, S.; Zhang, J.; Jia, C.; Luo, Z.; Zhang, L. Water soluble polymer binder with good mechanical property and ionic conductivity for high performance lithium sulfur battery. *Carbon* **2024**, *222*, 118807. [CrossRef]
62. Wen, Y.; Lin, X.; Sun, X.; Wang, S.; Wang, J.; Liu, H.; Xu, X. A biomass-rich, self-healable, and high-adhesive polymer binder for advanced lithium-sulfur batteries. *J. Colloid Interface Sci.* **2024**, *660*, 647–656. [CrossRef]
63. Zhang, T.; Mao, R.; Jiang, W.; Li, B.; Song, Z.; Liu, S.; Jian, X.; Hu, F. Dynamic cross-linking of zwitterionic polymer binder based on host-guest interactions for Li-S batteries with enhanced safety and electrochemical performance. *Nano Energy* **2023**, *114*, 108603. [CrossRef]
64. Reddy, B.R.S.; Ahn, J.-H.; Ahn, H.-J.; Cho, G.-B.; Cho, K.-K. Low-Cost and Sustainable Cross-Linked Polyvinyl Alcohol-Tartaric Acid Composite Binder for High-Performance Lithium-Sulfur Batteries. *ACS Appl. Energy Mater.* **2023**, *6*, 6327–6337. [CrossRef]
65. Gao, Q.; Shen, Z.; Guo, Z.; Li, M.; Wei, J.; He, J.; Zhao, Y. Metal Coordinated Polymer as Three-Dimensional Network Binder for High Sulfur Loading Cathode of Lithium-Sulfur Battery. *Small* **2023**, *19*, e2301344. [CrossRef] [PubMed]
66. Li, C.; Sun, Q.; Zhang, Q.; Xu, C.; Wang, S.; Ma, Y.; Shi, X.; Zhang, H.; Song, D.; Zhang, L. Multifunctional binder capable of promoting the reaction dynamics of wide temperature operable lithium-sulfur battery. *Chem. Eng. J.* **2023**, *455*, 140706. [CrossRef]
67. Pang, Z.; Zhang, H.; Ma, Y.; Song, D.; Shi, X.; Zhang, L.; Zhou, Y. Polyglutamic Acid Binder for High-Performance Lithium-Sulfur Batteries. *Coatings* **2022**, *12*, 1433. [CrossRef]
68. Wang, C.; Chen, P.; Wang, Y.; Chen, T.; Liu, M.; Zhang, M.; Fu, Y.; Xu, J.; Fu, J. Synergistic Cation-Anion Regulation of Polysulfides by Zwitterionic Polymer Binder for Lithium-Sulfur Batteries. *Adv. Funct. Mater.* **2022**, *32*, 2204451. [CrossRef]
69. Do, V.; Lee, S.H.; Jang, E.; Lee, J.-H.; Lee, J.-W.; Lee, J.T.; Cho, W.I. Aqueous Quaternary Polymer Binder Enabling Long-Life Lithium- Sulfur Batteries by Multifunctional Physicochemical Properties. *ACS Appl. Mater. Interfaces* **2022**, *14*, 19353–19364. [CrossRef]
70. Li, S.Z. Harnessing Heteropolar Lithium Polysulfides by Amphoteric Polymer Binder for Facile Manufacturing of Practical Li-S Batteries. *Small* **2022**, *18*, e2107109. [CrossRef]
71. Yang, Y.; Qiu, J.; Cai, L.; Liu, C.; Wu, S.; Wei, X.; Luo, D.; Zhang, B.; Yang, X.; Hui, K.N.; et al. Water-Soluble Trifunctional Binder for Sulfur Cathodes for Lithium-Sulfur Battery. *ACS Appl. Mater. Interfaces* **2021**, *13*, 33066–33074. [CrossRef]
72. Feng, J.; Yi, H.; Lei, Z.; Wang, J.; Zeng, H.; Deng, Y.; Wang, C. A three-dimensional crosslinked chitosan sulfate network binder for high-performance Li-S batteries. *J. Energy Chem.* **2021**, *56*, 171–178. [CrossRef]
73. Wang, R.-Y.; Kang, H.; Park, M.J. High-Capacity, Sustainable Lithium-Sulfur Batteries Based on Multifunctional Polymer Binders. *ACS Appl. Energy Mater.* **2021**, *4*, 2696–2706. [CrossRef]
74. Yoo, G.; Kim, S.; Chanthad, C.; Cho, M.; Lee, Y. Elastic rubber-containing multifunctional binder for advanced Li-S batteries. *Chem. Eng. J.* **2021**, *405*, 126628. [CrossRef]
75. Xie, Z.; Huang, Z.; Rong, M.; Zhang, M. Imparting high robustness and suppression ability of shuttle effect to sulfur cathode in the Li-S battery via a novel multifunctional binder. *Mater. Today Energy* **2020**, *18*, 100555. [CrossRef]
76. Luo, X.; Lu, X.; Chen, X.; Chen, Y.; Yu, C.; Su, D.; Wang, G.; Cui, L. A functional hyperbranched binder enabling ultra-stable sulfur cathode for high-performance lithium-sulfur battery. *J. Energy Chem.* **2020**, *50*, 63–72. [CrossRef]
77. Choi, S.; Kim, S.; Cho, M.; Lee, Y. Durable Conductive Webs as Multifunctional Binder for the High-Performance Lithium-Sulfur Battery. *ACS Appl. Energy Mater.* **2020**, *3*, 7825–7831. [CrossRef]
78. Liu, Z.; He, X.; Fang, C.; Forero, L.E.; Zhao, Y.; Fu, Y.; Feng, J.; Kostecki, R.; Balbuena, P.B.; Zhang, J.; et al. Reversible Crosslinked Polymer Binder for Recyclable Lithium Sulfur Batteries with High Performance. *Adv. Funct. Mater.* **2020**, *30*, 2003605. [CrossRef]
79. Kim, S.; Cho, M.; Chanthad, C.; Lee, Y. New redox-mediating polymer binder for enhancing performance of Li-S batteries. *J. Energy Chem.* **2020**, *44*, 154–161. [CrossRef]

80. Pham, C.V. Stabilization of Li-S batteries with a lean electrolyte via ion-exchange trapping of lithium polysulfides using a cationic, polybenzimidazolium binder. *Sustain. Energy Fuels* **2020**, *4*, 1180–1190. [CrossRef]
81. Kim, S. Multifunctional Chitosan-rGO Network Binder for Enhancing the Cycle Stability of Li-S Batteries. *Adv. Funct. Mater.* **2020**, *30*, 1907680. [CrossRef]
82. Cheng, X.-B.; Zhang, R.; Zhao, C.-Z.; Zhang, Q. Toward Safe Lithium Metal Anode in Rechargeable Batteries: A Review. *Chem. Rev.* **2017**, *117*, 10403–10473. [CrossRef] [PubMed]
83. Han, X.; Zhong, H.; Li, K.; Xue, X.; Wu, W.; Hu, N.; Lu, X.; Huang, J.; Xiao, G.; Mai, Y.; et al. Operando monitoring of dendrite formation in lithium metal batteries via ultrasensitive tilted fiber Bragg grating sensors. *Light-Sci. Appl.* **2024**, *13*, 24. [CrossRef] [PubMed]
84. Nam, H.; Song, W.; Chae, O.B. Advances in Coating Materials for Silicon-Based Lithium-Ion Battery Anodes. *Energies* **2024**, *17*, 4970. [CrossRef]
85. Ibrahem, S.L.; Nassar, M.Y.; Kader, S.M.A.E.; Fawzy, A.; Adam, M.S.S.; Masoud, E.M.; Khairy, M.; Sanad, M.M.S.; Mabrouk, E.M. Recent trending insights for enhancing silicon anode in lithium-ion battery via polymer coating. *Ionics* **2024**, *30*, 5879–5901. [CrossRef]
86. Saleem, M.; Lassi, U.; Srivastava, V.; Tuomikoski, S. A review of silicon-carbon anode materials: The role of precursor and its effect on lithium-ion battery performance. *J. Power Sources* **2025**, *641*, 236879. [CrossRef]
87. Li, J. An In Situ X-Ray Diffraction Study of the Reaction of Li with Crystalline Si. *J. Electrochem. Soc.* **2007**, *154*, A156. [CrossRef]
88. Saidi, N.M. Advancements in Silicon Anodes for Enhanced Lithium-Ion Batteries Performance: Innovations Toward Next-Gen Superbatteries. *Battery Energy* **2025**, *4*, e20240048. [CrossRef]
89. Huang, P.; Xie, C.; Huang, J.; Zhang, H.; Xu, M.; Chen, Y.; Chen, K.; Li, Y.; Xu, Q.; Peng, C.; et al. Robust cellulose levulinate ester as a novel non-ionic aqueous binder with high stability for lithium-ion batteries. *Chem. Eng. J.* **2025**, *521*, 166950. [CrossRef]
90. Ma, J.; Nan, H.; Yang, G.; Li, Z.; Wang, J.; Zhou, J.; Xue, C.; Wang, X.; Xu, S. Lithium-functionalized TEMPO-oxidized cellulose nanofiber as a novel binder and its impact on the ionic conductivity performance of lithium-ion batteries. *Cellulose* **2024**, *31*, 9681–9698. [CrossRef]
91. Yoon, J.; Han, G.; Cho, S.; Lee, C.; Lee, E.; Yoon, K.; Jin, H.-J. Microbial-Copolyester-Based Eco-Friendly Binder for Lithium-Ion Battery Electrodes. *ACS Appl. Polym. Mater.* **2023**, *5*, 1199–1207. [CrossRef]
92. Li, J.; Wang, Y.; Xie, X.; Kong, Z.; Tong, Y.; Xu, H.; Xu, H.; Jin, H. A novel multi-functional binder based on double dynamic bonds for silicon anode of lithium-ion batteries. *Electrochimica Acta* **2022**, *425*, 140620. [CrossRef]
93. Kim, W.-J.; Kang, J.G.; Kim, D.-W. Blood clot-inspired viscoelastic fibrin gel: New aqueous binder for silicon anodes in lithium ion batteries. *Energy Storage Mater.* **2022**, *45*, 730–740. [CrossRef]
94. Zhao, E.; Guo, Z.; Liu, J.; Zhang, Q.; Guo, Z.; Yang, Y.; Wang, H.; Wang, L. A low-cost and eco-friendly network binder coupling stiffness and softness for high-performance Li-ion batteries. *Electrochimica Acta* **2021**, *387*, 138491. [CrossRef]
95. Zhang, X.; Ge, X.; Shen, Z.; Ma, H.; Wang, J.; Wang, S.; Liu, L.; Liu, B.; Liu, L.; Zhao, Y. Green water-based binders for $LiFePO_4$/C cathodes in Li-ion batteries: A comparative study. *New J. Chem.* **2021**, *45*, 9846–9855. [CrossRef]
96. Wang, S.; Duan, Q.; Lei, J.; Yu, D.Y. Slime-inspired polyacrylic acid-borax crosslinked binder for high-capacity bulk silicon anodes in lithium-ion batteries. *J. Power Sources* **2020**, *468*, 228365. [CrossRef]
97. Hapuarachchi, S.N.S.; Wasalathilake, K.C.; Nerkar, J.Y.; Jaatinen, E.; O'mUllane, A.P.; Yan, C. Mechanically Robust Tapioca Starch Composite Binder with Improved Ionic Conductivity for Sustainable Lithium-Ion Batteries. *ACS Sustain. Chem. Eng.* **2020**, *8*, 9857–9865. [CrossRef]
98. Choi, D.; Choy, K.L. Spider silk binder for Si-based anode in lithium-ion batteries. *Mater. Des.* **2020**, *191*, 108669. [CrossRef]
99. Xu, H. A green-synthetic spiderweb-like Si@Graphene-oxide anode material with multifunctional citric acid binder for high energy-density Li-ion batteries. *Carbon* **2020**, *157*, 330–339. [CrossRef]
100. Phanikumar, V.V.N. A Sustainable Tamarind Kernel Powder Based Aqueous Binder for Graphite Anode in Lithium-Ion Batteries. *ChemistrySelect* **2020**, *5*, 1199–1208. [CrossRef]
101. Ndour, M.; Bonnet, J.-P.; Cavalaglio, S.; Lombard, T.; Safran, J.; Pau-Roblot, C.; Bonnet, V. Enzymatically demethylated pectins: From fruit waste to an outstanding polymer binder for silicon-based anodes of Li-ion batteries. *New J. Chem.* **2023**, *47*, 17499–17507. [CrossRef]
102. Wang, Z.; Xu, X.; Chen, C.; Huang, T.; Yu, A. Natural sesbania gum as an efficient biopolymer binder for high-performance Si-based anodes in lithium-ion batteries. *J. Power Sources* **2022**, *539*, 231604. [CrossRef]
103. Sandaruwan, R.D.L. White Latex: Appealing Green Alternative for PVdF in Electrode Manufacturing for Sustainable Li-Ion Batteries. *Langmuir* **2022**, *38*, 8934–8942. [CrossRef]
104. Chen, X.; Li, H.; Yan, Z.; Cheng, F.; Chen, J. Structure design and mechanism analysis of silicon anode for lithium-ion batteries. *Sci. China Mater.* **2019**, *62*, 1515–1536. [CrossRef]
105. Chen, S. Natural graphite anode for advanced lithium-ion Batteries: Challenges, Progress, and Perspectives. *Chem. Eng. J.* **2025**, *503*, 158116. [CrossRef]

106. Bindumadhavan, K.; Surendran, V.; Suriyakumar, S.; Rajasekharan, R.; Sivasubramanian, K.; Nair, S.; Shaijumon, M.M. Dual-functional trisiloxane as binder additive for high volume expansion Li-ion battery electrodes. *J. Energy Storage* **2024**, *77*, 109931. [CrossRef]
107. Nugraha, I.M.; Olchowka, J.; Brochon, C.; Flahaut, D.; Bousquet, M.; Cabannes-Boue, B.; Nuernberg, R.B.; Cloutet, É.; Croguennec, L. An Alternative Polymer Material to PVDF Binder and Carbon Additive in Li-Ion Battery Positive Electrode. *Adv. Sci.* **2024**, *11*, 2409403. [CrossRef]
108. Okonkwo, F.; Okonkwo, C. Assessment of poly(vinylidene fluoride) copolymer blends as recent binders for lithium-ion batteries with LiMn2O4 cathode. *J. Electrochem. Sci. Eng.* **2024**, *14*, 523–534. [CrossRef]
109. Xu, H.; Cao, R.; Li, J.; Xia, Y.; Wan, P.; Zhang, J.; Jin, H. A novel two-dimensional binder based on functionalized-graphene oxide for high performance Si anodes of Li ion batteries. *J. Energy Storage* **2024**, *102*, 114038. [CrossRef]
110. Li, S.; Gao, H.; Tan, J.; Qiu, Z.; Guo, X.; Yan, Y. Rigid-Flexible Integrated Polymer Binder via In Situ Esterification Cross-Linking for Si/C Anodes in Li-Ion Batteries. *ACS Appl. Mater. Interfaces* **2025**, *17*, 55338–55346. [CrossRef]
111. Saini, G.; Tan, M.; Stanzione, M.; Pancholi, K.; Kumar, H.; Walker, M.; Patterson, C.; Vassalli, M.; Naden, A.; Magdysyuk, O.; et al. Polyetherureas as aqueous binders for Li ion batteries. *GREEN. Chem.* **2025**, *28*, 318–325. [CrossRef]
112. Yang, M.; Rong, Z.; Li, X.; Yuan, B.; Zhang, W. Zwitterionic polymer as binder for $LiFePO_4$ cathodes in lithium-ion batteries. *Chem. Eng. J.* **2025**, *505*, 159332. [CrossRef]
113. Liu, X.; Zhang, M.; Peng, X.; Li, M.; Gao, X.; Feng, Y.; Chen, S.; Qu, X.; Zhang, X. Se-Se Bonds Involved Polyurethane-Based Binders for Enhanced Redox Kinetics in Lithium-Ion Batteries. *ACS Appl. Polym. Mater.* **2025**, *7*, 4019–4028. [CrossRef]
114. Kıgılcım, A.C.; Cetintasoglu, M.E.; Tokur, M.; Taskin, O.S.; Bulut, E.; Güzel, E. Versatile Spiro-Fluorene-Based Polymer Binder for Li-Ion Batteries. *ACS Appl. Polym. Mater.* **2025**, *7*, 2708–2715. [CrossRef]
115. Son, H.-J.; Reddy, B.; Na, H.-J.; Kim, J.-H.; Ahn, H.-J.; Ahn, J.-H.; Cho, G.-B.; Cho, K.-K. An elastic cross-linked polymeric binder for high-performance silicon/graphite composite anodes in lithium-ion batteries. *J. Alloys Compd.* **2025**, *1010*, 177724. [CrossRef]
116. Zhang, Z.; Ma, J.; Xiao, M.; Wang, S.; Huang, S.; Guo, H.; Han, D.; Meng, Y. Poly (Propylene Carbonate) with Extremely Alternating Structure Used as Binders for High-Loading Cathodes by Solvent-Free Method in High-Performance NCM811 Batteries. *Materials* **2024**, *17*, 5466. [CrossRef]
117. Weng, D.H.; Wu, L.Z.; He, Z.F.; Zhu, D.Y.; Li, Y.; Ma, B.; Liu, Q.; Chen, L.; Lin, Z.; Qiu, X. Robust self-healing ion-conductive interlocking dual-network binder based on gradient dynamic bonding for advanced SiO anodes in Li-Ion batteries. *Chem. Eng. J.* **2024**, *499*, 156360. [CrossRef]
118. Patra, A.; Matsumi, N. Densely Imidazolium Functionalized Water Soluble Poly(Ionic Liquid) Binder for Enhanced Performance of Carbon Anode in Lithium/Sodium-Ion Batteries. *Adv. Energy Mater.* **2024**, *15*, 2403071. [CrossRef]
119. Sun, X.; Lin, X.; Wen, Y.; Dong, F.; Guo, L.; Song, Z.; Yang, Z.; Liu, H.; Li, X.; Xu, X.; et al. A water-soluble binder in high-performance silicon-based anodes for lithium-ion batteries based on sodium carboxymethyl cellulose and waterborne polyurethane. *Green. Chem.* **2024**, *26*, 9874–9887. [CrossRef]
120. Gorji, P.; Ghahramani, M.; Haghighi-Yazdi, M. The electrochemical performance of $LiFePO_4$ electrodes based on polyurethane binder and carbon fiber current collector for lithium-ion batteries. *J. Energy Storage* **2024**, *99*, 113249. [CrossRef]
121. Lim, E.Y.; Kim, J.-O.; Lee, E.; Kwon, T.; Bin Park, J.; Ko, J.-W.; Cho, K.Y.; Lee, J.H. Interconnected Multifunctional Waterborne Polyurethane Binder for Structural Robustness of Si Anodes in Lithium-Ion Batteries. *Ind. Eng. Chem. Res.* **2024**, *63*, 12325–12335. [CrossRef]
122. Chen, B.; Zhang, Z.; Wu, C.; Huang, S.; Xiao, M.; Wang, S.; Guo, H.; Han, D.; Meng, Y. Aliphatic Polycarbonate-Based Binders for High-Loading Cathodes by Solvent-Free Method Used in High Performance $LiFePO_4$ | Li Batteries. *Materials* **2024**, *17*, 3153. [CrossRef]
123. Shen, J.; Zhang, S.; Wang, H.; Wang, R.; Hu, Y.; Mao, Y.; Wang, R.; Zhang, H.; Du, Y.; Fan, Y.; et al. Unlocking the potential of silicon anodes in lithium-ion batteries: A claw-inspired binder with synergistic interface bonding. *eScience* **2024**, *4*, 100207. [CrossRef]
124. Zhang, J.; Yan, L.; Zhao, Y.; Su, Y.; Sun, J.; Jiang, H.; Ma, T. A multifunctional supramolecular polymer binder with hard/soft phase interaction for Si-based lithium-ion batteries. *Nano Energy* **2024**, *125*, 109573. [CrossRef]
125. Li, S.; Zhang, X.; Chen, B.; Shi, Z.; Wu, S.; Wang, C.; Tong, Q.; Zhu, M.; Weng, J. Improving $LiFePO_4$ cathode stability in lithium-ion batteries by hybridizing activated tannic with PEDOT:PSS binders. *Electrochimica Acta* **2024**, *483*, 144037. [CrossRef]
126. Scheck, V.; Memm, M.; Hölzle, M.; Wohlfahrt-Mehrens, M. Improving the Fast Charging Capability of Lithium-Ion Battery Graphite Anodes by Implementing an Alternative Binder System. *J. Electrochem. Soc.* **2023**, *170*, 120514. [CrossRef]
127. Hwang, J.H.; Kim, E.; Lim, E.Y.; Lee, W.; Kim, J.; Choi, I.; Kim, Y.S.; Kim, D.; Lee, J.H.; Lee, J. A Multifunctional Interlocked Binder with Synergistic In Situ Covalent and Hydrogen Bonding for High-Performance Si Anode in Li-ion Batteries. *Adv. Sci.* **2023**, *10*, 2302144. [CrossRef]
128. Zhang, Z.; Han, D.; Xiao, M.; Wang, S.; Feng, Y.; Huang, S.; Meng, Y. New potential substitute of PVDF binder: Poly(propylene carbonate) for solvent-free manufacturing high-loading cathodes of $LiFePO_4$ | Li batteries. *Ionics* **2023**, *29*, 3895–3906. [CrossRef]

129. Kim, J.; Kim, G.; Park, Y.K.; Lim, G.; Kim, S.T.; Jung, I.H.; Kim, H. Structure-Performance Relationship of Aromatic Polymer Binder for Silicon Anode in Lithium-Ion Batteries. *Adv. Funct. Mater.* **2023**, *33*, 2303810. [CrossRef]
130. Azaki, N.J.; Ahmad, A.; Hassan, N.H.; Abdah, M.A.A.M.; Su'ait, M.S.; Ataollahi, N.; Lee, T.K. Poly(methyl methacrylate) Grafted Natural Rubber Binder for Anodes in Lithium-Ion Battery Applications. *ACS Appl. Polym. Mater.* **2023**, *5*, 4953–4965. [CrossRef]
131. Zhang, J.; Sun, J.; Zhao, Y.; Su, Y.; Meng, X.; Yan, L.; Ma, T. Prelithiated rigid polymer with high ionic conductivity as silicon-based anode binder for lithium-ion battery. *J. Colloid Interface Sci.* **2023**, *649*, 977–985. [CrossRef]
132. Ding, L.; Bagul, P.; Cui, L.; Oswald, S.; Pohle, B.; Leones, R.; Mikhailova, D. Graphite Anode Functionalized with a Gel Biopolymer Binder for Li-Ion Batteries Operating in a Broad Temperature Range. *ACS Appl. Energy Mater.* **2023**, *6*, 4404–4412. [CrossRef]
133. Yamazaki, S.; Tatara, R.; Mizuta, H.; Kawano, K.; Yasuno, S.; Komaba, S. High-performance SiO electrodes for lithium-ion batteries: Merged effects of a new polyacrylate binder and an electrode-maturation process. *Mater. Adv.* **2023**, *4*, 1637–1647. [CrossRef]
134. Park, H.G.; Son, Y.K.; Kim, J.; Lee, J.-S. Dual-effect-assisted cross-linkable poly(N-allyl-vinylimidazolium) • TFSI- as alternative electrode binder of lithium-ion battery. *Korean J. Chem. Eng.* **2023**, *40*, 504–511. [CrossRef]
135. Cai, Y.; Liu, C.; Yu, Z.; Ma, W.; Jin, Q.; Du, R.; Qian, B.; Jin, X.; Wu, H.; Zhang, Q.; et al. Slidable and Highly Ionic Conductive Polymer Binder for High-Performance Si Anodes in Lithium-Ion Batteries. *Adv. Sci.* **2023**, *10*, 2205590. [CrossRef]
136. Vauthier, S.; Alvarez-Tirado, M.; Guzmán-González, G.; Tomé, L.; Cotte, S.; Castro, L.; Guéguen, A.; Mecerreyes, D.; Casado, N. High-performance pyrrolidinium-based poly(ionic liquid) binders for Li-ion and Li-air batteries. *Mater. Today Chem.* **2023**, *27*, 101293. [CrossRef]
137. Oishi, A.; Tatara, R.; Togo, E.; Inoue, H.; Yasuno, S.; Komaba, S. Sulfated Alginate as an Effective Polymer Binder for High-Voltage LiNi0.5Mn1.5O4 Electrodes in Lithium-Ion Batteries. *ACS Appl. Mater. Interfaces* **2023**, *14*, 51808–51818. [CrossRef]
138. Zheng, F.; Tang, Z.; Lei, Y.; Zhong, R.; Chen, H.; Hong, R. PAAS-β-CDp-PAA as a high-performance easily prepared and water-soluble composite binder for high-capacity silicon anodes in lithium-ion batteries. *J. Alloys Compd.* **2023**, *932*, 167666. [CrossRef]
139. Yu, D.; Mu, L.; Feng, X.; Lin, F.; Madsen, L.A. Rigid-Rod Sulfonated Polyamide as an Aqueous-Processable Binder for Li-Ion Battery Electrodes. *ACS Appl. Energy Mater.* **2022**, *5*, 12531–12537. [CrossRef]
140. Gupta, A.; Badam, R.; Matsumi, N. Heavy-Duty Performance from Silicon Anodes Using Poly(BIAN)/Poly(acrylic acid)-Based Self-Healing Composite Binder in Lithium-Ion Batteries. *ACS Appl. Energy Mater.* **2022**, *5*, 7977–7987. [CrossRef]
141. Lee, H.; Preman, A.N.; Vo, T.N.; Lee, J.; Kim, I.T.; Ahn, S. In situ crosslinkable acrylic random copolymer binders for silicon anodes in lithium-ion batteries. *Int. J. Energy Res.* **2022**, *46*, 12565–12578. [CrossRef]
142. Liu, H.; Wu, Q.; Guan, X.; Liu, M.; Wang, F.; Li, R.; Xu, J. Ionically Conductive Self-Healing Polymer Binders with Poly(ether-thioureas) Segments for High-Performance Silicon Anodes in Lithium-Ion Batteries. *ACS Appl. Energy Mater.* **2022**, *5*, 4934–4944. [CrossRef]
143. Wang, Z.; Huang, T.; Liu, Z.; Yu, A. Dopamine-modified carboxymethyl cellulose as an improved aqueous binder for silicon anodes in lithium-ion batteries. *Electrochimica Acta* **2021**, *389*, 138806. [CrossRef]
144. Yu, L.-M.; Luo, Z.; Gong, C.-R.; Zheng, Y.-Q.; Zhou, Z.-X.; Zhao, H.; Xu, Y. Water-based binder with easy reuse characteristics for silicon/graphite anodes in lithium-ion batteries. *Polym. J.* **2021**, *53*, 923–935. [CrossRef]
145. Liu, H.; Chen, T.; Xu, Z.; Liu, Z.; Yang, J.; Chen, J. High-Safety and Long-Life Silicon-Based Lithium-Ion Batteries via a Multifunctional Binder. *ACS Appl. Mater. Interfaces* **2020**, *12*, 54842–54850. [CrossRef]
146. Ding, L.; Leones, R.; Omar, A.; Guo, J.; Lu, Q.; Oswald, S.; Nielsch, K.; Giebeler, L.; Mikhailova, D. Highly Efficient Multicomponent Gel Biopolymer Binder Enables Ultrafast Cycling and Applicability in Diverse Battery Formats. *ACS Appl. Mater. Interfaces* **2020**, *12*, 53827–53840. [CrossRef] [PubMed]
147. Das, P.; Zayat, B.; Wei, Q.; Salamat, C.Z.; Magdău, I.-B.; Elizalde-Segovia, R.; Rawlings, D.; Lee, D.; Pace, G.; Irshad, A.; et al. Dihexyl-Substituted Poly(3,4-Propylenedioxythiophene) as a Dual Ionic and Electronic Conductive Cathode Binder for Lithium-Ion Batteries. *Chem. Mater.* **2020**, *32*, 9176–9189. [CrossRef]
148. Tang, R.; Zheng, X.; Zhang, Y.; Ma, L.; Dong, Y.; Kong, G.; Wei, L. Highly adhesive and stretchable binder for silicon-based anodes in Li-ion batteries. *Ionics* **2020**, *26*, 5889–5896. [CrossRef]
149. Taskin, O.S.; Yuca, N.; Papavasiliou, J.; Avgouropoulos, G. Interconnected conductive gel binder for high capacity silicon anode for Li-ion batteries. *Mater. Lett.* **2020**, *273*, 127918. [CrossRef]
150. Gao, S.; Sun, F.; Brady, A.; Pan, Y.; Erwin, A.; Yang, D.; Tsukruk, V.; Stack, A.G.; Saito, T.; Yang, H.; et al. Ultra-efficient polymer binder for silicon anode in high-capacity lithium-ion batteries. *Nano Energy* **2020**, *73*, 104804. [CrossRef]
151. Jiang, S.; Hu, B.; Shi, Z.; Chen, W.; Zhang, Z.; Zhang, L. Re-Engineering Poly(Acrylic Acid) Binder toward Optimized Electrochemical Performance for Silicon Lithium-Ion Batteries: Branching Architecture Leads to Balanced Properties of Polymeric Binders. *Adv. Funct. Mater.* **2020**, *30*, 1908558. [CrossRef]

152. Wang, K.-L.; Chen, K.-T.; Yi, Y.-H.; Hung, Y.-H.; Tuan, H.-Y.; Horie, M. High-Performance Lithium Ion Batteries Combining Submicron Silicon and Thiophene-Terephthalic Acid-Conjugated Polymer Binders. *ACS Sustain. Chem. Eng.* **2020**, *8*, 1043–1049. [CrossRef]
153. Jolley, M.J.; Pathan, T.S.; Wemyss, A.M.; Prokes, I.; Moharana, S.; Wan, C.; Loveridge, M.J. Development and Application of a Poly(acrylic acid)-Grafted Styrene-Butadiene Rubber as a Binder System for Silicon-Graphite Anodes in Li-Ion Batteries. *ACS Appl. Energy Mater.* **2023**, *6*, 496–507. [CrossRef]
154. Ma, L.; Zhang, Y.; Wang, X.; Tang, R.; Zheng, X.; Dong, Y.; Kong, G.; Hou, Z.; Wei, L. Poly (acrylic acid-co-N-methylol acrylamide-co-butyl acrylate) copolymer grafted carboxymethyl cellulose binder for silicon anode in lithium ion batteries. *J. Appl. Electrochem.* **2020**, *51*, 131–141. [CrossRef]
155. Xia, Y.; Tong, J.; Lu, C.; He, X.; Gan, Y.; Huang, H.; Zhang, J.; Xia, X.; Zhang, W.; Xiao, Z.; et al. Natural okra gum as functional binder enables highly stable Lithium-Selenium batteries. *J. Phys. Chem. Solids* **2024**, *187*, 111865. [CrossRef]
156. Hu, C.; Wu, A.; Zhu, F.; Luo, L.; Yang, F.; Xia, G.; Wei, G.; Shen, S.; Zhang, J. Lithium-ion modified cellulose as a water-soluble binder for Li-O_2 battery. *Front. Energy* **2022**, *16*, 502–508. [CrossRef]
157. Zhao, L.; Dong, Q.; Wang, X.; Li, Z.; Shao, H.; Shen, Y.; Chen, L. Organic Mixed Ionic-Electronic Conductors as Multi-Functional Binders for Energy-Dense Carbon-Free Solid-State Batteries. *Batter. Supercaps* **2024**, *7*, e202400132. [CrossRef]
158. Lee, Y.-J.; Hong, S.-B.; Kim, D.-W. Exploring the use of butadiene rubbers as a binder in composite cathodes for all-solid-state lithium batteries. *J. Ind. Eng. Chem.* **2023**, *122*, 341–348. [CrossRef]
159. Hong, S.-B.; Lee, Y.-J.; Kim, U.-H.; Bak, C.; Lee, Y.M.; Cho, W.; Hah, H.J.; Sun, Y.-K.; Kim, D.-W. All-Solid-State Lithium Batteries: Li+-Conducting Ionomer Binder for Dry-Processed Composite Cathodes. *ACS Energy Lett.* **2022**, *7*, 1092–1100. [CrossRef]
160. Pan, Y.; Wu, X.; Yue, T.; Zhou, T.; Gao, P.; Gao, M.; Lei, T. Novel Copolymer Dispersant with Promoted Dispersibility of the LMFP Cathode Slurry for Boosting the Li-Ion Battery Performance. *ACS Appl. Energy Mater.* **2025**, *8*, 9430–9441. [CrossRef]
161. Kennedy, S.; Kim, J.-T.; Kim, J.; Lee, Y.M.; Phiri, I.; Ryou, S.-Y. Synergistic Effect of Dual-Ceramics for Improving the Dispersion Stability and Coating Quality of Aqueous Ceramic Coating Slurries for Polyethylene Separators in Li Secondary Batteries. *Batteries* **2022**, *8*, 82. [CrossRef]
162. Jeschull, F.; Zhang, L.; Kondracki, Ł.; Scott, F.; Trabesinger, S. Interphase formation with carboxylic acids as slurry additives for Si electrodes in Li-ion batteries. Part 1: Performance and gas evolution. *J. Phys.-Energy* **2023**, *5*, 025003. [CrossRef]
163. Wu, X.; Feng, J.; Amzil, S.; Peng, M.; Zhai, W.; Li, M.; Liu, X.; Cheng, Y.-J.; Xia, Y. A functional slurry additive for robust interphase and stabilized high-voltage nickel-rich cathodes in lithium-ion batteries. *Chem. Eng. J.* **2025**, *509*, 161446. [CrossRef]
164. Luo, Y.; Wang, L.; Wei, Z.; Huang, Q.; Deng, Y.; Zheng, Z. Cracking-Controlled Slurry Coating of Mosaic Electrode for Flexible and High-Performance Lithium-Sulfur Battery. *Adv. Energy Mater.* **2023**, *13*, 2203621. [CrossRef]
165. Kennedy, S.; Kim, J.-T.; Lee, Y.M.; Phiri, I.; Ryou, S.-Y. Upgrading the Properties of Ceramic-Coated Separators for Lithium Secondary Batteries by Changing the Mixing Order of the Water-Based Ceramic Slurry Components. *Batteries* **2023**, *8*, 64. [CrossRef]
166. Kim, K.T.; Kwon, T.Y.; Jung, Y.S. Scalable fabrication of sheet-type electrodes for practical all-solid-state batteries employing sulfide solid electrolytes. *Curr. Opin. Electrochem.* **2022**, *34*, 101026. [CrossRef]
167. Lee, J.; Lee, T.; Char, K.; Kim, K.J.; Choi, J.W. Issues and Advances in Scaling up Sulfide-Based All-Solid-State Batteries. *Acc. Chem. Res.* **2021**, *15*, 3390–3402. [CrossRef]
168. Gao, J.; Hao, J.; Gao, Y.; Sun, X.; Zhang, Y.; Song, D.; Zhao, Q.; Zhao, F.; Si, W.; Wang, K.; et al. Scalable wet-slurry fabrication of sheet-type electrodes for sulfide all-solid-state batteries and performance enhancement via optimization of Ni-rich cathode coating layer. *eTransportation* **2023**, *17*, 100252. [CrossRef]
169. Aguiló-Aguayo, N.; Hubmann, D.; Khan, F.U.; Arzbacher, S.; Bechtold, T. Water-based slurries for high-energy $LiFePO_4$ batteries using embroidered current collectors. *Sci. Rep.* **2020**, *10*, 5565. [CrossRef] [PubMed]
170. Zhu, B.; Zheng, T.; Xiong, J.; Shi, X.; Cheng, Y.-J.; Xia, Y. A Lithium-Ion Battery Cathode with Enhanced Wettability toward an Electrolyte Fabricated by a Fast Light Curing of Photoactive Slurry. *Energy Fuels* **2022**, *36*, 3313–3318. [CrossRef]
171. Copelli, S.; Dente, M.; Bozzano, G.; Barozzi, M. Simplified modeling and main constitutive parameters estimation for industrial emulsion copolymerization processes. *Chem. Eng. J.* **2018**, *335*, 988–1003. [CrossRef]
172. Zhao, B.; Yin, D.; Gao, Y.; Ren, J. Temperature-dependent rheological behavior of cathode slurry for lithium-ion battery under steady and dynamic tests. *Korea-Aust. Rheol. J.* **2023**, *35*, 191–201. [CrossRef]
173. Haghi, S.; Summer, A.; Bauerschmidt, P.; Daub, R. Tailored Digitalization in Electrode Manufacturing: The Backbone of Smart Lithium-Ion Battery Cell Production. *Energy Technol.* **2022**, *10*, 2200657. [CrossRef]
174. Dammala, P.K.; Dermenci, K.B.; Kathribail, A.R.; Yadav, P.; Van Mierlo, J.; Berecibar, M. A critical review of future aspects of digitalization next generation Li-ion batteries manufacturing process. *J. Energy Storage* **2023**, *74*, 109209. [CrossRef]
175. Manoharan, A.; Chong, J.J.; Choong, Z.J.; Lambert, S.; Gupta, R.K.; Chandra, D.; Jain, A.; Rao, A.; Sharma, A. Optimizing lithium-ion battery manufacturing with digitalization and AI-driven frameworks. *Int. J. Adv. Manuf. Technol.* **2025**, *142*, 1–37. [CrossRef]

176. Cui, X.; Garg, A.; Trung, N.T. Machine learning approach for solving inconsistency problems of Li-ion batteries during the manufacturing stage. *Int. J. Energy Res.* **2020**, *44*, 9194–9204. [CrossRef]
177. Yang, Z.; Huang, H.; Lin, F. Sustainable Electric Vehicle Batteries for a Sustainable World: Perspectives on Battery Cathodes, Environment, Supply Chain, Manufacturing, Life Cycle, and Policy. *Adv. Energy Mater.* **2022**, *12*, 2200383. [CrossRef]
178. Narimani-Qurtlar, A.; Sayyah, A.; Pakseresht, S.; Mostafaei, J.; Akbulut, H.; Cetinkaya, T.; Asghari, E.; Niaei, A. Investigating the environmental impacts of lithium-oxygen battery cathode production: A comprehensive assessment of the effects associated with oxygen cathode manufacturing. *J. Clean. Prod.* **2024**, *482*, 144199. [CrossRef]
179. Choudhary, N.; Clever, H.; Ludwigs, R.; Rath, M.; Gannouni, A.; Schmetz, A.; Hülsmann, T.; Sawodny, J.; Fischer, L.; Kampker, A.; et al. Autonomous Visual Detection of Defects from Battery Electrode Manufacturing. *Adv. Intell. Syst.* **2022**, *4*, 2200142. [CrossRef]
180. Duquesnoy, M.; Boyano, I.; Ganborena, L.; Cereijo, P.; Ayerbe, E.; Franco, A.A. Machine learning-based assessment of the impact of the manufacturing process on battery electrode heterogeneity. *Energy AI* **2021**, *5*, 100090. [CrossRef]
181. Chen, Y.-S.; Chang, J.-R.; Thotakura, Y.P.K.; Mohammad, A. A hybrid four-stage detection model to pre-identify the sustainable manufacturing process of Li-ion battery pack. *J. Supercomput* **2024**, *80*, 7624–7661. [CrossRef]
182. Lombardo, T.; Hoock, J.; Primo, E.N.; Ngandjong, A.C.; Duquesnoy, M.; Franco, A.A. Accelerated Optimization Methods for Force-Field Parametrization in Battery Electrode Manufacturing Modeling. *Batter. Supercaps* **2020**, *3*, 721–730. [CrossRef]
183. Pinilla, S.; Ryan, S.; McKeon, L.; Lian, M.; Vaesen, S.; Roy, A.; Schmitt, W.; Coleman, J.N.; Nicolosi, V. Additive Manufacturing of Li-Ion Batteries: A Comparative Study between Electrode Fabrication Processes. *Adv. Energy Mater.* **2023**, *13*, 2203747. [CrossRef]
184. Chen, K.; Deng, Z.; Luo, W.; Wei, S.; Tu, Z.; Wu, X. The Application of 3D Printing in Battery Manufacturing. *ChemSusChem* **2025**, *18*, e202500904. [CrossRef] [PubMed]
185. Huang, Z.; Cai, Y.; Zhang, S.; Wang, R.; Li, X.; Liu, Z. 3D aligned architectures for lithium batteries: Mechanism, design, and manufacture. *Energy Storage Mater.* **2025**, *75*, 103999. [CrossRef]
186. Park, S.; Shi, B.; Shang, Y.; Deng, K.; Fu, K. Structured Electrode Additive Manufacturing for Lithium-Ion Batteries. *Nano Lett.* **2022**, *22*, 9462–9469. [CrossRef] [PubMed]
187. Miranda, D.; Aliyev, T.; Kovacevic, L.; Voleti, S.; Lee, J.; Meehan, K.; So, M.C.; Dirlam, P.T. Lithium-Sulfur Batteries: 3D Printed Tools and Assembly Techniques for Repeatable Lab-Scale Coin Cell Manufacturing. *ACS Omega* **2025**, *11*, 1012–1018. [CrossRef] [PubMed]
188. Orisekeh, D.; Roh, B.-M.; Xiao, X. Solid-to-Solid Manufacturing Processes for High-Performance Li-Ion Solid-State Batteries. *Polymers* **2025**, *17*, 1788. [CrossRef]
189. Hu, J.; Jiang, Y.; Li, L.; Yu, Z.; Wang, C.; Gill, G.; Xiao, J.; Cavagnaro, R.J.; Kuo, L.-J.; Asmussen, R.M.; et al. A Lithium Feedstock Pathway: Coupled Electrochemical Extraction and Direct Battery Materials Manufacturing. *ACS Energy Lett.* **2022**, *7*, 2420–2427. [CrossRef]
190. Xiao, Y.; Turcheniuk, K.; Narla, A.; Song, A.-Y.; Ren, X.; Magasinski, A.; Jain, A.; Huang, S.; Lee, H.; Yushin, G. Electrolyte melt infiltration for scalable manufacturing of inorganic all-solid-state lithium-ion batteries. *Nat. Mater.* **2021**, *20*, 984–990. [CrossRef]
191. Jeong, M.H.; Jeong, J.H.; Youn, H.J.; Jung, S.Y.; Ahn, K.H. High-Speed Li-Ion Battery Manufacturing Process Applying the Dewatering Concept. *Ind. Eng. Chem. Res.* **2024**, *63*, 4408–4419. [CrossRef]
192. Zhou, R.; Ong, H.L.; Fu, Y.; Mamlouk, M.; Cheng, C. Solvent-Free Manufacturing of Lithium Iron Phosphate Cathodes via Binder Fibrillation for Li-Ion Batteries. *Energy Technol.* **2025**, *13*, 2500649. [CrossRef]
193. Liu, Y.; Gong, X.; Podder, C.; Wang, F.; Li, Z.; Liu, J.; Fu, J.; Ma, X.; Vanaphuti, P.; Wang, R.; et al. Roll-to-roll solvent-free manufactured electrodes for fast-charging batteries. *Joule* **2023**, *7*, 952–970. [CrossRef]
194. Verdier, N.; Foran, G.; Lepage, D.; Prébé, A.; Aymé-Perrot, D.; Dollé, M. Challenges in Solvent-Free Methods for Manufacturing Electrodes and Electrolytes for Lithium-Based Batteries. *Polymers* **2021**, *13*, 323. [CrossRef]
195. Wang, M.J.; Carmona, E.; Gupta, A.; Albertus, P.; Sakamoto, J. Enabling lithium-free manufacturing of pure lithium metal solid-state batteries through in situ plating. *Nat. Commun.* **2020**, *11*, 5201. [CrossRef]
196. Díaz-Ramírez, M.C.; Ferreira, V.J.; García-Armingol, T.; López-Sabirón, A.M.; Ferreira, G. Battery Manufacturing Resource Assessment to Minimise Component Production Environmental Impacts. *Sustainability* **2020**, *12*, 6840. [CrossRef]
197. Carrère, T.; Khalid, U.; Baumann, M.; Bouzidi, M.; Allard, B. Carbon footprint assessment of manufacturing of synthetic graphite battery anode material for electric mobility applications. *J. Energy Storage* **2024**, *94*, 112356. [CrossRef]
198. Yang, N.; Li, Z.; He, L. Recovery of battery-grade products from mixed spent $LiFePO_4$/$LiMn_2O_4$ cathodes via slurry electrolysis. *Sep. Purif. Technol.* **2023**, *317*, 123859. [CrossRef]
199. Zuo, A.; Feng, H.; Yuan, T.; Xu, L.; Shu, K.; Tian, J.; Luo, Y.; Xue, K. One-step Fe/Li separation via slurry electrolysis from spent $LiFePO_4$ batteries and iron-based composite formation for photocatalytic tetracycline degradation. *Sep. Purif. Technol.* **2025**, *377*, 134207. [CrossRef]
200. Wang, Y.; Fei, R.; Yuan, Z.; Li, Y.; Zhang, H.; Li, J. Low-carbon emitting Fe-cycle recovery of battery-grade $FePO_4$ from biogas slurry for Li-battery application. *Chem. Eng. J.* **2024**, *496*, 154131. [CrossRef]

201. Bruno, M.; Lassila, L.L.; Francia, C.; Santasalo-Aarnio, A.; Fiore, S. Technical, economic and environmental analysis of production scraps direct recycling from lithium-ion battery manufacturing. *Clean. Environ. Syst.* **2025**, *20*, 100386. [CrossRef]
202. Yao, M.; Sano, H.; Ando, H. Recycling Compatible Organic Electrode Materials Containing Amide Bonds for Use in Rechargeable Batteries. *Polymers* **2023**, *15*, 4395. [CrossRef] [PubMed]
203. Wu, S.; Huang, C.; Shen, W.; Long, X.; Ye, Z.; Qiu, J.; Xie, L.; Zhou, W.; Zhang, S.; Wei, X.; et al. A water-soluble binder for recyclable lithium-ion batteries. *Nat. Sustain* **2026**, *9*, 575–584. [CrossRef]
204. Panda, P.K.; Sung, J.-I.; Li, J.; Hsieh, C.-T. Lithium-Metal Batteries with Ternary Cathode-Supported NASICON-Type Composite Solid Electrolytes Enabling High-Rate Capability and Excellent Cyclic Performance. *ACS Appl. Energy Mater.* **2026**, *9*, 5007–5015. [CrossRef]
205. Charrier, S. Additive manufacturing by binder jetting of thick electrode for Li-ion battery. *J. Power Sources* **2026**, *670*, 239420. [CrossRef]